

# Computation of turbulent natural convection in rectangular enclosures with an algebraic flux model

K. HANJALIĆ† and S. VASIĆ‡

†Lehrstuhl für Strömungsmechanik Universität Friedrich-Alexander, Erlangen-Nürnberg, Germany  
(on leave from the University of Sarajevo, Bosnia Herzegovina)

‡Mašinski fakultet, University of Sarajevo, Bosnia Herzegovina

(Received 20 May 1992)

**Abstract**—The paper reports on the computation of laminar and turbulent natural convection in rectangular enclosures with aspect ratios of 1 and 5 with simple- and mixed-boundary conditions in the range of  $Ra$  numbers from  $10^4$  to  $10^{12}$ . A form of the algebraic model for the turbulent heat flux vector  $\theta u$ , with the low  $Re$  number  $k$ - $\epsilon$  transport equations, found earlier to predict well some cases of external free convection, gave satisfactory results in all considered cavity flows. Parallel computations with several variants of eddy diffusivity  $k$ - $\epsilon$  model failed to produce a consistent quality of results, indicating a necessity to employ a higher order model which departs from the isotropic eddy diffusivity concept. It was found that the effects of both the mean temperature- and mean velocity-gradients on the dynamics of turbulent heat transport should be accounted for, particularly in cases with more complex boundary conditions.

## 1. INTRODUCTION

NATURAL convection in a two-dimensional cavity is one of many examples of turbulent flows whose geometrical simplicity conceals the full complexity of the real flow pattern. In spite of a significant practical importance in many engineering and environmental applications and numerous research reports in literature, the problem has not been fully understood as yet. There are still no reliable models or correlations which can be used with certainty for the prediction of heat transfer in cavities, in particular if the boundary conditions are non-standard.

A common practice to establish experimentally the heat transfer correlation in form  $Nu = f(Ra, Pr, A, \dots)$  has so far not produced a consensus even for the simple 'clean' cases, such as cavities with side heating and cooling. This is best illustrated by the variety of relationships available in literature both for the laminar and turbulent convection (e.g. Gebhart *et al.* [1]). For cavities with more complex boundary conditions every new situation requires a different relationship, as shown by Kirkpatrick and Bohn [2] and others. Hence, in spite of a dose of skepticism towards the numerical solutions, partly justified by still present uncertainties in both the numerical accuracy and in modeling turbulence under the dominance of buoyancy, it is likely that the numerical computations of field properties by a flexible code with an advanced turbulence model will be used more and more in the future to predict the natural convection in unknown situations.

A major feature of the natural convection in confined domains is a recirculating motion induced by

buoyancy forces due to heat transfer on the enclosing non-adiabatic walls. As pointed out by Ostrach [3], two distinct flow patterns can be discerned: boundary layers forming along the enclosure walls and the encircled rotating core. The flow in the core region is influenced by the boundary conditions only indirectly through the interaction with the surrounding boundary layers and can take various patterns in the form of one or more rolls, depending on the wall conditions and the value of the  $Ra$  number. In case of higher  $Ra$  numbers, turbulence will be generated in the boundary layers and diffuse into the core, but the structure of turbulence and the mechanisms which govern the transport of heat and momentum in these two regions will have essentially different scales. Mutual interaction between the wall boundary layers and the core region and consequent modifications of both patterns is the major reason for limited success in attempting to derive scaling laws applicable to cavities with different boundary conditions and aspect ratios.

The mentioned features and others place a particular demand on turbulence models for natural convection which are expected to depict all important turbulent processes in wall boundary layers, cavity corners and in the core region, as well as the interactions at the zones interfaces.

Two-dimensional cavities are not of a significant practical interest *per se*, because all geometries of practical relevance are three-dimensional. They have been a subject of detailed investigation over the years mainly because of their geometrical simplicity and supposed convenience for experimental verification. They also serve as a basis for testing the ideas for devising and improving the turbulence models aimed

## NOMENCLATURE

$A$	aspect ratio, $H/W$	$U_i$	mean velocity
$B_{ij}$	buoyancy parameter, $\beta g_i (k/\varepsilon)^2 (\partial T/\partial x_j)$	$U_1, U$	horizontal mean velocity
$C$	empirical coefficients	$U_2, V$	vertical mean velocity
CV	abbreviation for control volume	$\overline{u_i u_j}$	turbulent stress tensor
$g_i$	gravitational acceleration $(0, -g, 0)$	$V_b$	buoyant velocity, $\sqrt{(\beta g \Delta T H)}$
$G$	buoyancy production of turbulence energy	$W$	enclosure width
$H$	enclosure height	$x_i$	coordinate
$k$	turbulence kinetic energy	$x_1, x$	horizontal coordinate
$L$	enclosure length	$x_2, y$	vertical coordinate
$Nu$	local Nusselt number at the wall, $-(H/\Delta T)(\partial T/\partial x_n)$	$y^+$	dimensionless coordinate normal to the wall, $x_n U_i/\nu$ .
$\overline{Nu}$	averaged Nusselt number at the wall, $\int_0^1 Nu \, d(y/H)$	Greek symbols	
$P$	production of turbulence energy due to mean rate of strain	$\beta$	coefficient of thermal expansion
$Pr$	Prandtl number	$\Delta T$	difference between hot- and cold-wall temperatures
$R$	ratio of mechanical-to-thermal time scale of turbulence	$\varepsilon$	rate of dissipation of turbulence energy
$Re_i$	turbulence Reynolds number, $k^2/\nu\varepsilon$	$\tilde{\varepsilon}$	isotropic part of $\varepsilon$
$Ra$	Rayleigh number, $\beta g \Delta T H^3 Pr/\nu^2$	$\eta$	empirical coefficient
$Ra_W$	Rayleigh number, $\beta g \Delta T W^3 Pr/\nu^2$	$\overline{\theta^2}$	temperature variance
$T$	temperature	$\theta u_i$	turbulent heat flux vector
$T_{bulk}$	reference bulk temperature	$\nu$	kinematic molecular viscosity
$T_c$	temperature of the cold wall	$\nu_i$	kinematic turbulent viscosity
$T_h$	temperature of the hot wall	$\xi$	empirical coefficient
$T^*$	non-dimensional temperature excess, $(T - T_c)/\Delta T$	$\rho$	fluid density
$u_i$	fluctuating velocity	$\tau_w$	wall shear stress
		$\phi_0$	empirical coefficient
		$\Phi$	general symbol for dependent variable.

at application to more general and practically relevant three-dimensional confined natural convection. In fact, experimental evidence indicates that effects of three-dimensionality are often discernible even in strictly two-dimensional geometries and they are probably the major cause for a noticeable sensitivity of confined buoyancy driven flows to the enclosure configuration and frequently reported disagreement and non-repeatability of the measured results.

All these factors, as well as the appearance of a well organized coherent structure discernible particularly in cases with heating from below, pose a serious challenge to the modeling, and are reasons for an evident distrust in the numerical computations of natural convection in interiors. To this, one may add a strong coupling and mutual feed-back between the density (temperature, species concentration) and velocity fluctuating fields as well as a need to account for molecular effects. The latter are known to remain important in some areas of the flow (e.g. the initial regions of the boundary layers along the vertical walls) even through the bulk  $Ra$  number may far exceed the critical values for the appearance of turbulent regime.

Accurate description of turbulent natural convection in an enclosure seems to require at least the second-moment closure level in order to ensure predictions of non-standard behavior pertinent to the buoyancy driven flows. Such is, e.g. a turbulent transport of heat in regions where the mean temperature has close-to-uniform profile or gradient directed opposite to the turbulent flux vector (counter-gradient diffusion). Other requirements include the prediction of a switch from laminar-to-turbulent regime at the appropriate local  $Ra$  numbers (not necessarily the transition phenomenon itself, which, of course, is not tractable by the Reynolds averaging). This is important in some new applications such as crystal growth, cooling of the electronic circuits or of nuclear reactors. In the first case, the appearance of even small instabilities and any turbulence may be detrimental to the crystal quality. These and similar cases are sensitive tests for the low  $Re$  number modifications of the turbulence models.

In comparison with the isothermal flows dominated by shear or pressure gradient, the application of second-moment closure methods for buoyancy driven flows pose much more uncertainty because of a need

to model a number of unknown correlations representing the interactions between the fluctuating velocity and temperature field. Proposals for these correlations have been published in literature (e.g. Launder [4]) but their verification has been so far limited only to some simple flows such as boundary layer at a heated vertical plate (e.g. Peeters and Henkes [5]). For that reason, but also because of an increasing number of equations to be solved which, for complex three-dimensional geometries with irregular boundaries, may pose a formidable problem, we have focused our attention on a simpler level of modeling which ultimately reduces to a form of an algebraic turbulent flux model. Turbulence scales have been obtained by the solution of the transport equations for  $k$  and  $\varepsilon$  with low  $Re$  number modifications.

The work described here will be limited to two-dimensional cavities. The paper first discusses two cases of rectangular cavities, both with side heating and cooling and adiabatic top and bottom walls: a square cavity and a tall cavity with a 5 : 1 aspect ratio. The influence of mixed boundary conditions are discussed in an example of a square cavity with one side wall and bottom wall heated and the other side wall and top wall cooled. All cases will be considered for the range of  $Ra$  numbers between  $10^9$  and  $10^{12}$ , i.e. around the laminar-to-turbulent transition. It is believed that this range of  $Ra$  number represents the most severe test for the turbulence modeling. Also, some computations have been performed with different  $Pr$  numbers. The accuracy of the applied numerical code and grid refinement will be illustrated by several examples of the computation of laminar natural convection in a square cavity for  $10^4 < Ra < 10^9$ .

## 2. PREVIOUS WORK AND RELEVANT REFERENCES

Over the past decade a number of reports appeared in the literature on the computations of turbulent natural convection in two-dimensional enclosures. Fraikin *et al.* [6], Markatos and Pericleous [7], Ozoe *et al.* [8], Thompson *et al.* [9], Fusegi and Farouk [10] and Nobile *et al.* [11] used the standard high  $Re$  number  $k$ - $\varepsilon$  model and employed wall functions for the treatment of wall boundary conditions. Several anomalies have been detected in the computed results demonstrating the inadequacy of the employed models. For example, Markatos and Pericleous (who, like some other earlier authors, omitted the buoyancy generation terms in both the  $k$ - and  $\varepsilon$ -equations) obtained the Nusselt numbers which are much larger than found by experiments. The computations of Ozoe *et al.* and of Fusegi and Farouk show unrealistic double peaks in the profile of the kinetic energy close to the wall. Thompson found that the eddy viscosity has a maximum value in the middle of the cavity and employed artificial damping functions to eliminate this erroneous behavior. Fraikin *et al.* (who con-

sidered the case with horizontal walls having a linear temperature distribution) and Nobile *et al.* considered only relatively small  $Ra$  numbers up to  $10^{10}$ .

Recognizing the fact that in buoyant flows along non-adiabatic vertical walls the buoyancy effects are significant very close to the wall where the flow is also affected by molecular transport, several authors computed the natural convection in enclosures by employing the low  $Re$  number variant of the  $k$ - $\varepsilon$  model, e.g. Betts *et al.* [12], Ince and Launder [13], Davidson [14], Giel and Schmidt [15], Hanjalić and Vasić [16] and Henkes *et al.* [17]. The latter models seem to be generally more successful than the standard  $k$ - $\varepsilon$  version, though most authors reported a need to introduce additional modifications to the model in order to achieve acceptable agreement with experiments. Even the same model with slightly different damping functions can produce noticeable effects. A case in point is the low  $Re$  number model of Jones and Launder [18], which serves as a basis of most computations, including the present ones. A variant of this model as proposed by Launder and Sharma [19], which differs from the original mainly in the form of the damping function  $f_\mu$  in the eddy diffusivity, produces the laminar-to-turbulent transition and the predictions of the field properties in the transition region notably closer to the experimental observations than the original model. An important effect upon the solution has also been the definition of the dependent variable in the dissipation equation (and its boundary conditions), which enters the expression for the eddy diffusivity. A choice of  $\tilde{\varepsilon} = \varepsilon - \nu(\partial k^{1/2}/\partial x_n)^2$  instead of  $\varepsilon$  will generate a higher eddy viscosity close to a wall and, consequently, a faster transition and higher Nusselt numbers. These seemingly small differences may be the source of inconsistencies in the quality of results reported by some authors. For example, Ozoe *et al.* [8] reported that the application of Jones and Launder model led to a collapse of turbulence even though the  $Ra$  number was sufficiently high. Another source of disagreement is the triggering of the turbulence field in case of vertical heated plate, which may produce quite a different outcome. Some other specific features of models applied by various authors will be outlined in conjunction with the discussion of our results.

## 3. LAMINAR CONVECTION: NUMERICAL METHOD AND GRID OPTIMIZATION

The numerical computations were carried out by means of a control volume numerical code based on the TEACH algorithm. Both the uniform and non-uniform grids in either staggered or collocated arrangements have been employed but the final computations presented here were carried out by employing a mildly non-uniform, staggered grid. Two implicit numerical schemes were tested in parallel: the line-by-line (LBL) iterative method with the three-diagonal matrix algorithm TDMA and Stone's strongly-implicit procedure (SIP). The latter method, with a

modification of Perić [20], was found to be more efficient and has subsequently been used for further computations.

Tests of the numerical code were carried out on several selected test cases which were computed with different schemes (including the upwind- and central-differencing of the convective terms), and with different grid sizes and distributions. We first discuss briefly the case of laminar free convection in a square cavity with differentially heated vertical walls kept at either constant temperature or heat flux (or mixed), and with adiabatic horizontal walls. A number of available publications on experimental, analytical or numerical investigations of this flow case (some of them also covering the turbulent regime) renders it as very suitable for test purposes. Besides, contrary to more complex cases with mixed-boundary conditions, here a 'clean' situation is generated in which the temperature gradient is perpendicular to the gravitational vector. The slightest temperature difference causes an instantaneous fluid motion. Heat transfer mode depends on the overheat ratio and on the intensity of the consequent buoyancy force. At small buoyancy, in spite of fluid motion, the dominant heat transfer from the warm to the cold wall through the fluid in between occurs by conduction. As the wall temperature difference increases, the convective mechanism becomes more important and gradually takes over the dominant role in the heat exchange. For the  $Ra$  number (defined with the cavity width and warm-cold wall temperature difference) greater than  $10^4$  laminar boundary layers form on each vertical wall. At a sufficiently high  $Ra$  number—of the order of  $10^{10}$ —the flow regime in the boundary layers changes from laminar to turbulent, but at the initial parts of the walls and in starting corners it may remain laminar even though the bulk  $Ra$  number may be well above the transition limit. A peculiarity of this flow case is the formation of an almost stagnant, vertically stratified, central core.

For testing the numerical procedure and for studying the influence of grid spacing and distribution, we adopted here the well known 'benchmark' numerical

solutions of Vahl Davis [21] for  $Ra = 3.5 \times 10^5$  to serve as a reference case. More recent computations of Hortmann *et al.* [22], carried out for  $Ra = 10^4$ ,  $10^5$  and  $10^6$  with a multi-grid method and with an impressive grid refinement up to  $640 \times 640$  CV, generated very accurate solutions which can be employed for reliable testing of the applied numerical method and grid dependence studies. In addition, the present results have been compared with some of the available experimental data.

The above described numerical method was applied to several sets of elementary control volumes up to  $80 \times 80$  CV, but here, for illustration, a comparison will be presented for only the two selected cases with relatively coarse numerical grids, i.e.  $20 \times 20$  and  $40 \times 40$  in uniform and non-uniform arrangements. Also, the influence of upwind- and central-differencing scheme is presented. The computed values of the average Nusselt number at the vertical walls for various cases are shown in Table 1, together with the relative differences in regard to the reference value  $Nu = 6.494$ , which was obtained by the interpolation of Vahl Davis solutions for three  $Ra$  numbers, i.e.  $10^4$ ,  $10^5$  and  $10^6$ . As could be seen, the non-uniform grid with  $40 \times 40$  CV with both the upwind- and central-differencing of the convective terms yielded the solutions which agree with the selected reference value within 1%. The result with a coarser grid of  $20 \times 20$  non-uniformly spaced CV causes a discrepancy within a tolerable 4%, while a uniform grid with the same number of CV produces an unacceptable error of over +18%. For comparison, some results of computations of Poleshaev [23] for the same geometry (deduced from graphs  $Nu = C Ra^d$ ), for  $20 \times 20$  CV, uniformly distributed, for three different treatments of convective terms have also been presented in Table 1. As shown, his computations with the upwind-differencing gave a value of  $Nu$  that differs from the Vahl Davis result by  $-10.7\%$  (note the opposite sign in comparison with ours!), while the central-differencing gave much larger values, and close to our result obtained with upwind-differencing. The reason for such discrepancy between the results of Poleshaev and

Table 1. Comparison of numerical grids and differencing schemes for the convection terms,  $Ra = 3.5 \times 10^5$

No. of CV grid scheme		40 × 40		20 × 20			
		Non-uniform		Uniform			
		Upwind	Central	Upwind	Upwind	Central	Samarski
1	$Nu$	6.539	6.556	6.756	7.674		
	$\Delta Nu/Nu^*$	0.69%	0.95%	4.03%	18.2%		
2	$Nu$				5.80	7.70	6.75
	$\Delta Nu/Nu^*$				-10.7%	18.6%	3.94%

1 Hanjalić and Vasić.

2 Poleshaev (1989).

\* Reference value:  $Nu^* = 6.494$  (interpolated from the results of Vahl Davis, 1983).

present computations lies probably in other differences in the applied numerical schemes and will not be elaborated here. It is, however, pertinent to note that in both cases a coarse uniform grid with  $20 \times 20$  CV performs unsatisfactorily. A much better agreement for the same grid seems to have been achieved by means of a higher order scheme of Samarski, as reported by Poleshaev.

The computations with a non-uniform grid with  $40 \times 40$  CV for three other different  $Ra$  numbers,  $10^4$ ,  $10^5$  and  $10^6$ , yielded results which were in excellent agreement with both the Vahl Davis and Hortmann *et al.* solutions, as illustrated in Table 2. Hence, this grid configuration and the upwind differencing scheme were subsequently adopted as fully adequate for the computation of laminar flows in rectangular domains. It was noticed, however, that the solutions become more dependent on the fineness of the numerical grid as the  $Ra$  number increases. The critical factor is the number of grid points between the wall and the velocity maximum. It was found that the grid-independent solution for laminar convection requires at least six grid points in this domain. The same type of grid also proved to be adequate for the computation of turbulent flows, but only if the high  $Re$  number model with wall functions was used. However, since this approach appeared to be inadequate due to the uncertainties in specifying the wall functions, the computations of turbulent regimes were carried out by means of a low  $Re$  number turbulence model which requires a grid squeezed in the near-wall region, and, consequently, at least 60 CV in one direction.

Table 2 presents a quantitative comparison of several characteristic parameters in a square cavity for three values of  $Ra$ , computed by our code and with the bench-mark computations of Vahl Davis and Hortmann *et al.* As seen, all parameters agree very well. The differences between the averaged Nusselt numbers are in all cases smaller than 1%. It is inter-

esting to note that the above results agree within 5% with the correlation of Berkovsky and Polevikov (as cited in ref. [1])

$$Nu = 0.18 \left( \frac{Ra Pr}{0.2 + Pr} \right)^{0.29} \quad (1)$$

recommended for  $1 < A < 2$  and a wide range of  $Pr$  and  $Ra$  numbers.

Further tests have also been carried out by comparing the details of the computed velocity- and temperature-profiles with the available experimental results. As an illustration, we present here the comparison of the computed and measured results for two cases. The first case is a water filled cavity of aspect ratio  $A = 0.5$  investigated experimentally by Ozoe *et al.* [24]. The vertical side walls were kept at constant temperatures of 14.8 and 7.8°C, respectively, so that  $Ra = 1.52 \times 10^8$ . All other walls were isolated. Ozoe *et al.* measured the horizontal and vertical velocity components at several cross-sections along both vertical and horizontal walls, while the temperatures were measured by thermocouples. Figure 1 shows the measured and computed profiles of the vertical velocity at four selected cavity heights. Computations, obtained with a non-uniform grid with  $120 \times 60$  CV show excellent agreement with the measurements for all profiles in the lower part of the cavity, while some discrepancies were noticed in the upper region. As pointed out by Ozoe *et al.* [24], it was noticed during the experiment that the temperature of the hot wall increased gradually from 14.7 to 15°C causing a higher fluid heating and, consequently, higher maximum velocities than obtained by computations. It is interesting to note that the numerical computations of Ozoe *et al.* [8] gave a noticeable disagreement with their own experimental data even in the lower part of the cavity, which could be attributed to the coarseness of the applied grid ( $48 \times 24$  CV). Our computation with a

Table 2. Comparison of characteristic parameters for a square cavity for three values of  $Ra$  number

$Ra$	$10^4$			$10^5$			$10^6$		
	1	2	3	1	2	3	1	2	3
$U_{max}$ (m s <sup>-1</sup> )	0.159	0.162	0.162	0.357	0.347	0.347	0.658	0.646	0.648
$y/H$	0.835	0.823	0.826	0.858	0.855	0.855	0.869	0.850	0.850
$V_{max}$ (m s <sup>-1</sup> )	0.195	0.196	0.196	0.682	0.686	0.686	2.187	2.194	2.205
$x/W$	0.122	0.119	0.120	0.069	0.066	0.066	0.042	0.038	0.039
$Nu_{max}$	3.550	3.528	3.531	7.681	7.717	7.720	17.974	17.925	17.536
$y/H$	0.143	0.144	0.146	0.085	0.081	0.082	0.037	0.038	0.039
$\bar{Nu}$	2.240	2.243	2.245	4.508	4.519	4.522	8.857	8.800	8.825
$\frac{\Delta \bar{Nu}}{\bar{Nu}} \dagger$	-0.147%		0.078%	-0.244%		0.058%	0.651%		0.286%
$\frac{\Delta \bar{Nu}}{\bar{Nu}} \ddagger$	-0.225%	-0.078%		-0.302%	-0.058%		0.364%	-0.285%	

1, present results; 2, Vahl Davis (1983); 3, Hortmann *et al.* (1989).

† Normalized with solutions of Vahl Davis.

‡ Normalized with solutions of Hortmann *et al.*

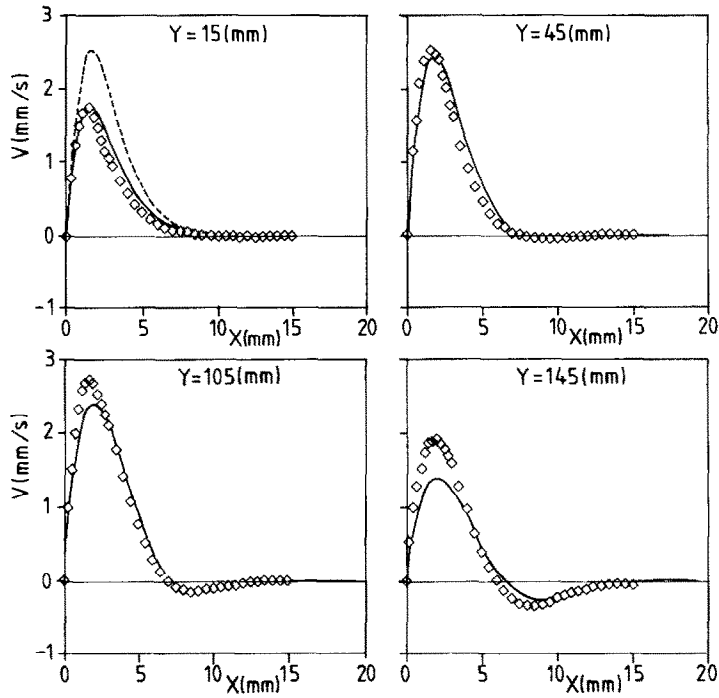


FIG. 1. Vertical velocity profiles close to the hot wall for a cavity with  $A = 0.5$ ,  $Ra = 1.52 \times 10^8$  and  $Pr = 9.17$ :  $\diamond$ —experiments of Ozoë *et al.* [24], --- computations of Ozoë *et al.* [8], ——— present computations.

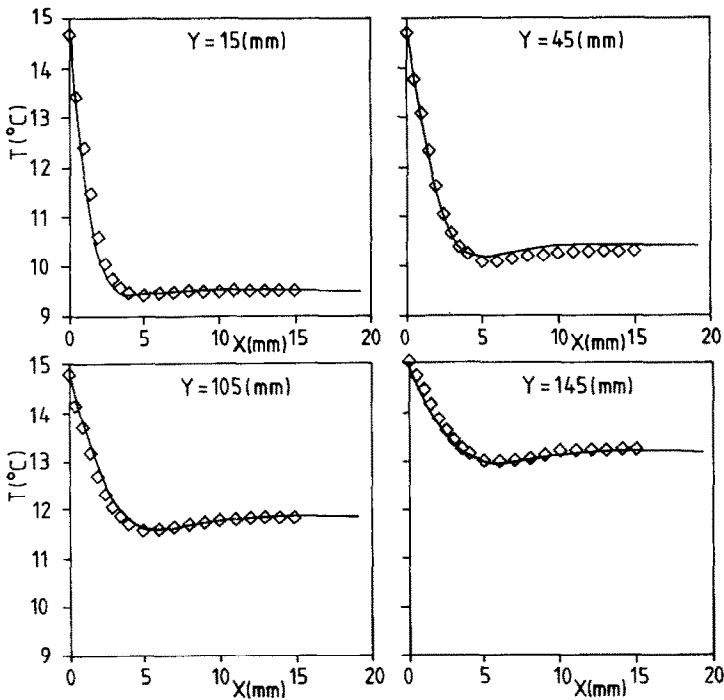


FIG. 2. Temperature profiles close to the hot wall for a cavity with  $A = 0.5$ ,  $H = 0.16$  m,  $Ra = 1.52 \times 10^8$  and  $Pr = 9.17$ :  $\diamond$ —experiments of Ozoë *et al.* [24], --- computations of Ozoë *et al.* [8], ——— present computations.

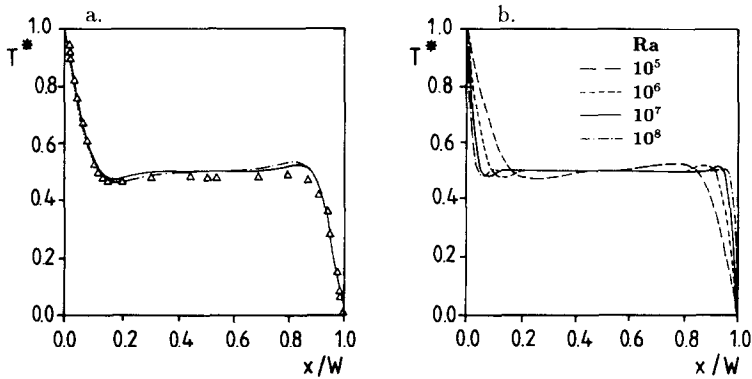


FIG. 3. Normalized temperature profile at cavity midheight: (a)  $Ra = 3.5 \times 10^5$ ,  $\Delta$ —experiments of Bajorek and Lloyd [25], ——— computations for adiabatic top and bottom walls, - - - computations for conductive top and bottom walls; (b) influence of  $Ra$  number.

coarser grid of  $60 \times 30$  CV also gave some differences in the values and positions of maximum velocity because of the insufficient resolution in this region, though overall agreement is not much different from the above described results with the fine mesh. The profiles of the temperature showed, however, an excellent agreement with the measurements at all tested cross-sections, as illustrated in Fig. 2.

The second case which served for comparison is the experiment of Bajorek and Lloyd [25]. Figure 3 presents the comparison between the computed and measured normalized temperature profiles at the cavity midheight for  $Ra = 3.5 \times 10^5$ . Because of the relatively small dimensions of the cavity, the experiment was not well controlled and some unspecified heat losses were detected causing a small discrepancy between the results in the cavity center. The same reason seems to have caused a considerable difference between the measured and computed distributions of the Nusselt number along the vertical walls as shown in Fig. 4. In order to check the influence of possible

departure from adiabatic conditions at the horizontal walls, the same case was computed with horizontal walls assumed as being ideally conductive. As seen in Fig. 4(a), the agreement is much better. It seems, therefore, that realistic boundary conditions at the horizontal walls would bring the agreement to the desired accuracy. Figure 4(b) illustrates the influence of the  $Ra$  number.

#### 4. TURBULENT CONVECTION: GOVERNING EQUATIONS AND TURBULENCE MODEL

In the course of investigations reported here, several different levels of turbulence modeling have been analyzed, starting with the simple, standard  $k-\epsilon$  model, modified accordingly to account for buoyancy effects in all equations. The aim was to find the level of modeling which can give acceptable agreement with experimental data for several families of buoyancy-dominated flows with different boundary conditions, but still remain simple enough to be employed for

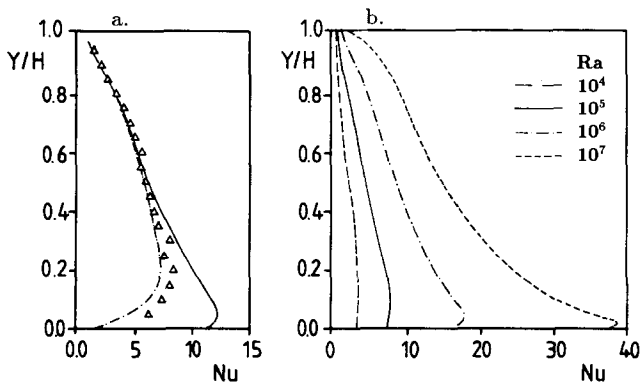


FIG. 4. Distribution of Nusselt number along the vertical wall: (a)  $\Delta$ —experiments of Bajorek and Lloyd [25], ——— computations for adiabatic top and bottom walls, - - - computations for conductive top and bottom walls; (b) influence of  $Ra$  number.

the solution of more complex three-dimensional flows with irregular boundaries. The highest modeling level considered was the differential stress/flux model, which requires the solution of the equations for all second-order turbulence correlations representing the turbulent flux of momentum, heat and species. However, this model was applied only to the two cases of unsteady penetrative convection of a mixed layer into stably stratified fluid, when the heat flux gradient is aligned with—but opposed to—the gravity vector. These two cases represent examples of pure buoyancy-generated turbulence, and conclusions drawn in regard to the performance of various models in these two cases served as a basis for the choice of the model for a further use in computation of natural convection in cavities. More details are described in Hanjalić and Vasić [26].

#### 4.1. Algebraic heat flux model (AFM)

For the case of two-dimensional turbulent natural convection in simple- and multiple-zone reactangular domains with arbitrary conditions it was found that satisfactory results require the treatment of turbulent heat flux vector at least in the algebraic form in order to account for major effects recorded by experiments. As will be shown later, the cavity aspect ratio is an influential parameter. It appeared that a natural convection in square- and low-aspect ratio cavities with thermally active side walls can be reasonably well predicted by a simple low  $Re$  number  $k$ - $\varepsilon$  eddy diffusivity model. However, the same model applied to the computation of natural convection in a tall cavity produces too late transition and consequently erroneous temperature and velocity fields in most parts of the central region. The disagreement with experiments increases as the aspect ratio increases. The algebraic model produced on the whole a better overall agreement irrespective of the aspect ratio and  $Ra$  number.

A further justification for adopting the algebraic model came from the computations of the mentioned cases of penetrative convection. Even the standard eddy diffusivity model for the vertical heat flux component produces results of quality close to that obtained with the full second moment model (and in close agreement with experiments) provided a modification was introduced to 'relax' the direct proportionality of the flux to the mean temperature gradient. This can conveniently be done by introducing the variable turbulent Prandtl number, as it was done earlier by Gibson and Launder [27], and which, in fact, represents a form of an algebraic flux model.

The basis of the adopted model (with Boussinesq approximation applied only to eliminate the fluctuating density in terms of temperature fluctuation) are the modeled differential transport equations for the turbulent heat flux  $\overline{\theta u_i}$ , and the temperature variance  $\overline{\theta^2}$ . These equations can be truncated (e.g. Launder [4]), to yield a set of implicit algebraic expressions

$$\overline{\theta u_i} = -\phi_\theta \frac{k}{\varepsilon} \left[ \overline{u_i u_j} \frac{\partial T}{\partial x_j} + (1 - C_{\theta 2}) \overline{\theta u_j} \frac{\partial U_i}{\partial x_j} + (1 - C_{\theta 3}) \beta g_i \overline{\theta^2} \right] \quad (2)$$

$$\overline{\theta^2} = -C_\theta'' \frac{k}{\varepsilon} \overline{\theta u_j} \frac{\partial T}{\partial x_j} \quad (3)$$

where  $\phi_\theta$ ,  $C_\theta''$ ,  $C_{\theta 2}$  and  $C_{\theta 3}$  are empirical coefficients, to be discussed later.

The turbulence kinetic energy  $k$  and its dissipation rate  $\varepsilon$  are used to describe the evolution of the turbulence field and to define the turbulence scale. The transport equations for these two variables were solved in the following form:

$$\frac{D(\rho k)}{Dt} = D_k + \rho P + \rho G - \rho \varepsilon \quad (4)$$

$$\frac{D(\rho \varepsilon)}{Dt} = D_\varepsilon + C_{\varepsilon 1} \rho P \frac{\varepsilon}{k} + C_{\varepsilon 3} \rho G \frac{\varepsilon}{k} - C_{\varepsilon 2} f_\varepsilon \rho \frac{\varepsilon \tilde{\varepsilon}}{k} + E \quad (5)$$

where

$$P = -\overline{u_i u_j} \frac{\partial U_i}{\partial x_j}; \quad G = -\beta g_i \overline{\theta u_i};$$

$$E = 2\mu \frac{\mu_i}{\rho} \left( \frac{\partial^2 U_i}{\partial x_j \partial x_k} \right)^2; \quad \tilde{\varepsilon} = \varepsilon - \nu \left( \frac{\partial k^{1/2}}{\partial x_n} \right)^2;$$

$$D_\Phi = \frac{\partial}{\partial x_j} \left( C_\Phi \rho \frac{k}{\varepsilon} \overline{u_j \theta} \frac{\partial \Phi}{\partial x_k} + \mu \frac{\partial \Phi}{\partial x_j} \right).$$

$P$  and  $G$  stand for the turbulence energy production by strain and buoyancy, respectively,  $E$  accounts for molecular effects in the production of  $\varepsilon$ , while  $D_\Phi$  denotes the total diffusion of the variable  $\Phi$ , in which the turbulent contribution was modeled by the general gradient expression.

In expressions (2) and (3) the coefficients  $\phi_\theta$  and  $C_\theta''$  are generally functions dependent on the turbulence energy unbalance. Here, adopted truncation approximations  $\phi_\theta$  and  $C_\theta''$  take the following forms, respectively

$$\phi_\theta = \left[ C_{\theta 1} + \frac{1}{2} \left( \frac{P+G}{\varepsilon} - 1 \right) + \frac{1}{4R} \left( \frac{P_\theta}{\varepsilon_\theta} - 1 \right) \right]^{-1} \quad (6)$$

$$C_\theta'' = 2 \left( \frac{P+G}{\varepsilon} - 1 + R^{-1} \right)^{-1} \quad (7)$$

where  $R$  represents the ratio of the thermal-to-mechanical turbulence scale.

The expression (3) can be used to eliminate  $\overline{\theta^2}$  from equation (2). By introducing for convenience a generalized form of 'buoyancy parameter'†

† Note that  $B_k$  is an asymmetric second rank tensor and that the first index denotes the direction of the gravitation vector.

$$B_{ik} = \beta g_i \left( \frac{k}{\varepsilon} \right)^2 \frac{\partial T}{\partial x_k} \quad (8)$$

the turbulent heat flux vector can be written in the form of a recurrent expression

$$\overline{\theta u_i} = -\phi_\theta \left[ \frac{k}{\varepsilon} \left( \overline{u_i u_j} \frac{\partial T}{\partial x_j} + \overline{v \theta u_i} \frac{\partial U_i}{\partial x_j} \right) - \eta B_{ij} \overline{\theta u_j} \right] \quad (9)$$

where

$$\xi = (1 - C_{\theta 2}); \quad \eta = C_\theta^\theta (1 - C_{\theta 3}). \quad (10)$$

Expression (2) can also be written explicitly for each flux component in the form of a general eddy viscosity expression in which the heat flux is proportional to both the mean temperature- and mean velocity-gradients. This form may prove to be computationally more convenient than the implicit expression (2). In this case, the mutual coupling between the flux components is accounted for through variable turbulent Prandtl-Schmidt numbers which take the form of second rank tensors as described by Hanjalić and Vasić [26].

In the present work we deal only with rectangular two-dimensional cavities. For the selected coordinate system with  $x_1$  in the horizontal direction and  $x_2$  denoting the vertical direction upwards so that  $g_i(0, -g, 0)$ , it follows that  $B_{11} = B_{12} = 0$ . The algebraic expressions for the horizontal and vertical heat flux read now

$$\begin{aligned} \overline{\theta u_1} = -\phi_\theta \frac{k}{\varepsilon} \left[ \overline{u_1^2} \frac{\partial T}{\partial x_1} + \overline{u_1 u_2} \frac{\partial T}{\partial x_2} \right. \\ \left. + \xi \left( \overline{\theta u_1} \frac{\partial U_1}{\partial x_1} + \overline{\theta u_2} \frac{\partial U_1}{\partial x_2} \right) \right] \quad (11) \end{aligned}$$

$$\begin{aligned} \overline{\theta u_2} = -\frac{\phi_\theta}{1 - \phi_\theta \eta B_{22}} \left\{ \frac{k}{\varepsilon} \left[ \overline{u_1 u_2} \frac{\partial T}{\partial x_1} + \overline{u_2^2} \frac{\partial T}{\partial x_2} \right. \right. \\ \left. \left. + \xi \left( \overline{\theta u_1} \frac{\partial U_2}{\partial x_1} + \overline{\theta u_2} \frac{\partial U_2}{\partial x_2} \right) \right] - \eta B_{21} \overline{\theta u_1} \right\}. \quad (12) \end{aligned}$$

As can be seen, both expressions contain all gradients of the mean temperature and mean velocity. Excluding the cavity corners, streamwise gradients are substantially smaller than the lateral ones. Nevertheless, it has been noticed that streamwise gradients have an influence upon the prediction of flux components, especially in tall cavities and with mixed boundary conditions. This is particularly true for the flux component which is aligned with the gravitation vector—here  $\overline{\theta u_2}$ —which governs directly the buoyant production of the kinetic energy  $G$ . Although found to be usually less than one-third of the shear production in the outer layer, the buoyant production becomes important in the inner wall layer and its adequate modeling is essential for accurate predictions of the whole flow domain.

Expressions (11) and (12) contain the components of the Reynolds stress tensor. They can also be expressed

in the algebraic form. However, having in mind a possible extension of the model to more complex and three-dimensional geometries, we explored simpler options. It is expected that in buoyancy dominated flows an accurate prediction of individual normal stress components may not be of crucial importance as compared with the heat flux vector. As can be inferred from the measurements of Tsuji *et al.* [28] in a boundary layer along a heated vertical plate, the ratio of the vertical normal stress and kinetic energy remains reasonably constant around the value of 1.1 (within 15%) over the whole layer cross-section, while the ratio of the lateral component and kinetic energy varies between 0.25 in the inner region to about 0.4 in the outer region. These findings give grounds to adopt  $\overline{u_i u_i} / k = \text{const.}$  for the evaluation of individual normal stresses appearing in expressions (11) and (12). For the same reason, the shear stress was evaluated from the standard eddy viscosity expression

$$\overline{u_i u_j} = \frac{2}{3} k \delta_{ij} - \nu_t \left( \frac{\partial U_i}{\partial x_j} + \frac{\partial U_j}{\partial x_i} \right),$$

with  $\nu_t = C_\mu f_\mu (k^2 / \varepsilon)$ .

The forms of the two functions of turbulence  $Re$  number are adopted from Launder and Sharma [19]

$$f_\mu = \exp \left[ \frac{-3.4}{\left( 1 + \frac{Re_t}{50} \right)^2} \right] \quad f_\varepsilon = 1 - 0.3 \exp(-Re_t^2). \quad (13)$$

The empirical coefficients in the  $k$  and  $\varepsilon$  equations are those which have been generally adopted for isothermal flows. The exception is the coefficient  $C_{\varepsilon 3}$  for which no general consensus has as yet been achieved. Values from 0 to  $C_{\varepsilon 1}$  have been proposed by various authors. It is obvious that the zero value has no physical justification since in pure buoyancy-generated turbulence like in a stagnant fluid heated from below, this is the only remaining source of  $\varepsilon$ . Without this term,  $\varepsilon$  would decay very fast and there will be no provision in the model to describe the turbulent energy sink. More recently (e.g. Ince and Launder [13]) there has been a tendency to lump the buoyancy- and shear-production in the source of  $\varepsilon$  equation together with a single coefficient, i.e.  $C_{\varepsilon 3} = C_{\varepsilon 1}$ , which implies that both the shear- and buoyancy-production play the same role in the energy decay dynamics. This proposal looks attractive because the number of coefficients in the model is reduced by one. However, our tests with the penetrative convection of a mixed layer in unstable conditions showed that the results are sensitive to the choice of  $C_{\varepsilon 3}$  and the best agreements with experiments for two earlier mentioned cases have been obtained with  $C_{\varepsilon 3} \approx 0.5 C_{\varepsilon 1}$ . In the case of vertical heated surfaces the predictions are less sensitive to the choice of  $C_{\varepsilon 3}$  presumably because the shear production dominates the turbulence dynamics. We

adopted, therefore,  $C_{\varepsilon 3} = 0.8$  for all cases in conjunction with the algebraic flux model (AFM).

The coefficients in the heat flux expression (2) were adopted mainly from literature (e.g. Launder [4]) with some modifications. A strict application of the algebraic modeling will imply the computation of the coefficients  $\phi_\theta$  and  $C_\theta''$  in the function of the production and dissipation of the turbulence energy and temperature variance, as given by equations (6) and (7). In line with our goal to arrive at the simplest form of the model which will still yield satisfactory predictions of the considered range of cases, we explored the behavior of these two functions. An inspection of available data for a boundary layer along a vertical heated plate revealed a large discrepancy. The data of Tsuji *et al.* [28] suggest in the outer region, for  $y^+ > 100$ , that  $(P+G)/\varepsilon$  is about 1, while in the inner region the ratio decreases fast to become even negative very close to the wall because of large, negative shear production. These authors claim that the turbulence energy source here is dominated by the pressure straining extraction of thermal energy from the mean motion. This term is usually neglected on the grounds of continuity requirements if the fluid is regarded as incompressible. Although these findings may have a justification in a region very close to a heated plate with a large overheat ratio, it is hard to accept that this effect is so significant. On the other hand, the computations of To and Humphrey [29] and our own, yield a ratio of  $(P+G)/\varepsilon$  between 1.5 and 2 in the outer region, suggesting a high surplus of turbulence energy which is being convected downstream and diffused towards the inner region. Of course, none of the mentioned models accounts for the pressure strain source of the kinetic energy. Similarly, the ratio of  $P_\theta/\varepsilon_\theta$  of Tsuji *et al.* reaches a value of about 1.8 at  $y^+ \approx 15$ , to drop sharply both in the inner and outer regions. Based on our computations of a flow along a heated vertical plate, which does not account for the turbulence energy generation by the pressure straining, we found that—with an exception very close to the wall—both  $\phi_\theta$  and  $C_\theta''$  assume reasonably constant values. Figure 5 shows  $\phi_\theta$  across the boundary layer at a heated vertical plate, computed with  $C_{\theta 1} = 3.0$  and with the assumption that  $P_\theta = \varepsilon_\theta$ . On the basis of these findings we adopted  $\phi_\theta = 0.28$  and  $C_\theta'' = 1$ . It is interesting to note that for local equilibrium of the kinetic energy equation  $(P+G) = \varepsilon$  the latter value implies that the ratio of the thermal-to-mechanical turbulence scale  $R = 0.5$ . This is very close to the experimental results of Tsuji *et al.* [28] who found that  $R$  remains almost uniform with values between 0.55 and 0.6 in a large portion of the boundary layer cross-section for  $15 < y^+ < 300$ . If one assumes that  $(P+G)/\varepsilon$  and  $P_\theta/\varepsilon_\theta = 1$  the adopted value of  $\phi_\theta = 0.28$  will require that  $C_{\theta 1} = 3.57$ , which is close to 3.7 as suggested by Tavoularis and Corrsin [30].

As for other coefficients, we adopted  $C_{\theta 2} = C_{\theta 3} = 0.4$  so that  $\xi = \eta = 0.6$ . With this set of coeffi-

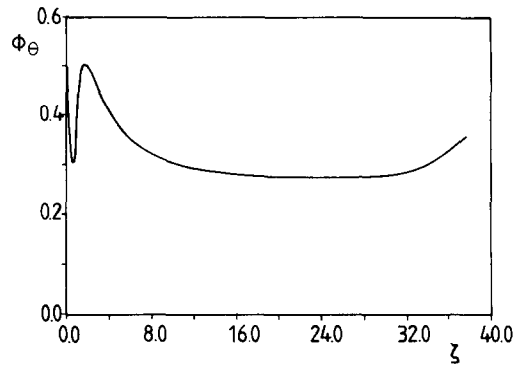


FIG. 5. Computed variation of  $\phi_\theta$  across the boundary layer at a heated vertical wall.

cients the model produced results of a consistent quality and in acceptable agreement with available experiments for the case of free convection along a heated vertical plate, in a mixed layer heated from below or cooled from above (Hanjalić and Vasić [26]), as well as in rectangular cavities with different boundary conditions and aspect ratio. A summary of the coefficients is given in Table 3.

#### 4.2. Simpler models

For comparison, some cases have also been computed by applying several variants of simpler models. The first is the standard eddy diffusivity low  $Re$  number  $k-\varepsilon$  model in which the turbulent heat flux is expressed in the form of simple gradient diffusion, i.e.  $\overline{\theta u_i} = -(\nu_t/\sigma_\theta)(\partial T/\partial x_i)$  (hence denoted as ‘SGD’ model) with the same form of  $k$  and  $\varepsilon$  equations. The second model follows Ince and Launder [13] and employs the generalized gradient diffusion hypothesis (denoted as ‘GGD’) for the heat flux vector in form  $\overline{\theta u_i} = -C_\theta(k\overline{u_i u_j}/\varepsilon)(\partial T/\partial x_j)$  with the value of  $C_\theta = 0.15$ , as recommended by the authors to satisfy the horizontal shear flows with main velocity and temperature gradients in vertical direction. The third model considered is the same as the previous, but with a neglect of the streamwise temperature gradient in the expression for  $\overline{\theta u_i}$ , and denoted for that reason as ‘partially’ generalized gradient hypotheses (‘PGGD’).<sup>†</sup> Ince and Launder reported that the application of the Launder–Sharma [19] model with

Table 3. Summary of coefficients

$C_k$	$C_\theta$	$C_\varepsilon$	$C_{\varepsilon 1}$	$C_{\varepsilon 2}$	$C_{\varepsilon 3}$	$\xi$	$\eta$	$\phi$
0.20	0.11	0.15	1.44	1.92	0.8	0.6	0.6	0.28

<sup>†</sup> In fact, the expression for  $\overline{\theta u_2}$  which enters the buoyant production of  $k$  in the paper of Ince and Launder [13] contains only the lateral gradient indicating that the authors have neglected the streamwise gradient as unimportant. The matter is discussed in more detail later.

$\tilde{\epsilon}$  in the eddy viscosity formula produced too high a  $Nu$  number in an infinite cavity. The introduction of the GGD hypothesis, but also of the wall correction term of Yap (quoted in ref. [13]) in the  $\tilde{\epsilon}$ -equation to reduce the excessive slope of the length scale in the wall region, brought the results into a very good agreement with experiments. We have tested the GGD and PGGD both with and without Yap correction. The former models are denoted as GGD+Y and PGGD+Y, respectively.

## 5. RESULTS AND DISCUSSION

We consider first the two cases of rectangular cavities with side heating and cooling and adiabatic horizontal walls. The first geometry is a square cavity and the second is a tall cavity with an aspect ratio of 5:1. In both cases the vertical walls were assumed to be isothermal. The considered fluid was air and the covered  $Ra$  numbers between  $10^{10}$  to  $10^{12}$ . In order to investigate the implication of the Boussinesq hypothesis, we adopted first a small temperature difference of only 2 K so that the covered  $Ra$  number range was achieved by varying the cavity size. Later we also tested some cases with larger temperature differences up to 46 K. No reliable experimental data are yet available in the literature for field properties in a square cavity which could serve as a basis for verification of the computations. For this purpose we have used mainly the correlations for the Nusselt number on the side walls, the computations of other authors and the measured data for field properties of Cheesewright and co-workers [31–33] for the 5:1 cavity.

### 5.1. Square cavities with thermally active vertical walls

We present first some results of computation for an air-filled square cavity of dimensions  $7.8 \times 7.8$  m. The temperature of the warm wall was  $T_h = 30^\circ\text{C}$  and of the cold wall  $T_c = 10^\circ\text{C}$ , yielding a value of Rayleigh number  $Ra = 10^{12}$ . With these parameters, the case corresponds closely to a simple, but real situation that can be encountered in space heating (e.g. double glazing). Computations were performed for a non-uniform numerical grid with  $120 \times 120$ ,  $120 \times 80$  and  $100 \times 80$  CV, squeezed in the regions next to the vertical walls so that at least 30 points fall within the wall boundary layers. The coarsest mesh produced only a marginal difference in the mean  $Nu$  number. The computations were started with some initial turbulence field. No special triggering was found necessary and provided the initial ratio of  $k$  and  $\epsilon$  was within a range which ensured that the initial eddy viscosity is about 10 times higher than the molecular one, turbulent solutions were obtained at all considered  $Ra$  numbers greater than  $5 \times 10^{10}$ . A different ('less turbulent') solution was detected at  $Ra = 10^{12}$  in the case of very low initial level of turbulence, indicating a possibility of non-unique solutions, as found also by Henkes *et al.* [17]. In this case the transition was

delayed and its position could not be determined with certainty. The computations required a much longer time to converge and did not produce conclusive evidence of possible bifurcation. These results will be omitted from further consideration and we will discuss only the fully turbulent results which showed a full consistency for a range of initial conditions.

A selection of computed results is presented in Figs. 6–9. We start the discussion with the fully turbulent case for  $Ra = 10^{12}$ . Figures 6(a)–(c) illustrating the streamlines, temperature- and turbulence-contours, show clearly that the main motion of the fluid occurs within the thin boundary layers along the vertical walls, while in the rest of the cavity space a strong density stratification is established and the fluid flows slowly in the horizontal direction from the cold towards the warm wall. Along the vertical walls the fluid velocity reaches a maximum slightly downstream from the midheight of each wall. Secondary vortices, which usually form at smaller  $Ra$  numbers in the bottom left and upper right corners, are in this case hardly detectable; they are very elongated and drawn towards the corners as indicated by the negative values of the vertical velocity components.

The normalized temperature profiles, shown in Fig. 7(a) at five different horizontal positions, collapse almost fully into one curve showing a high level of similarity except for the slight departure at the cross-section very close to the warm wall. A blow-up of the profiles very close to the wall confirms the fulfillment of the adiabatic conditions at the horizontal walls.

The influence of the  $Ra$  number around the transition is illustrated in Figs. 7(b) and 8(a)–(c). As seen, at  $Ra = 10^{10}$  the turbulence collapses and the computations produced a practically laminar solution. A small but persisting level of turbulence was obtained for  $Ra = 5 \times 10^{10}$ , but typical turbulent solutions appeared only at  $Ra$  around  $10^{12}$ . This is best illustrated in Fig. 8 which shows the profiles of the vertical mean velocity, turbulence kinetic energy and eddy viscosity for a range of  $Ra$  numbers. In all cases, the turbulence field is characterized by the concentration of turbulence in the upper left and lower right wall regions. The rest of the flow field is almost non-turbulent, confirming a strong stable stratification in the central region of the cavity. Even in the case of highest considered  $Ra$  number of  $10^{12}$ , which is well above the critical value, the intensity of turbulence is not high, with the maximum ratio of eddy-to-molecular viscosity at the midplane of only about 140. These features illustrate best that reliable predictions could only be expected with turbulence models which incorporate adequate low  $Re$  number modifications.

The distribution of Nusselt number along the warm wall for the three different  $Ra$  numbers ( $10^{10}$ – $10^{12}$ ) are shown in Fig. 9 (along the cold wall identical, but anti-symmetric profiles have been obtained). As expected the largest values are obtained in the lower corner where the fluid, cooled by the cold wall, comes

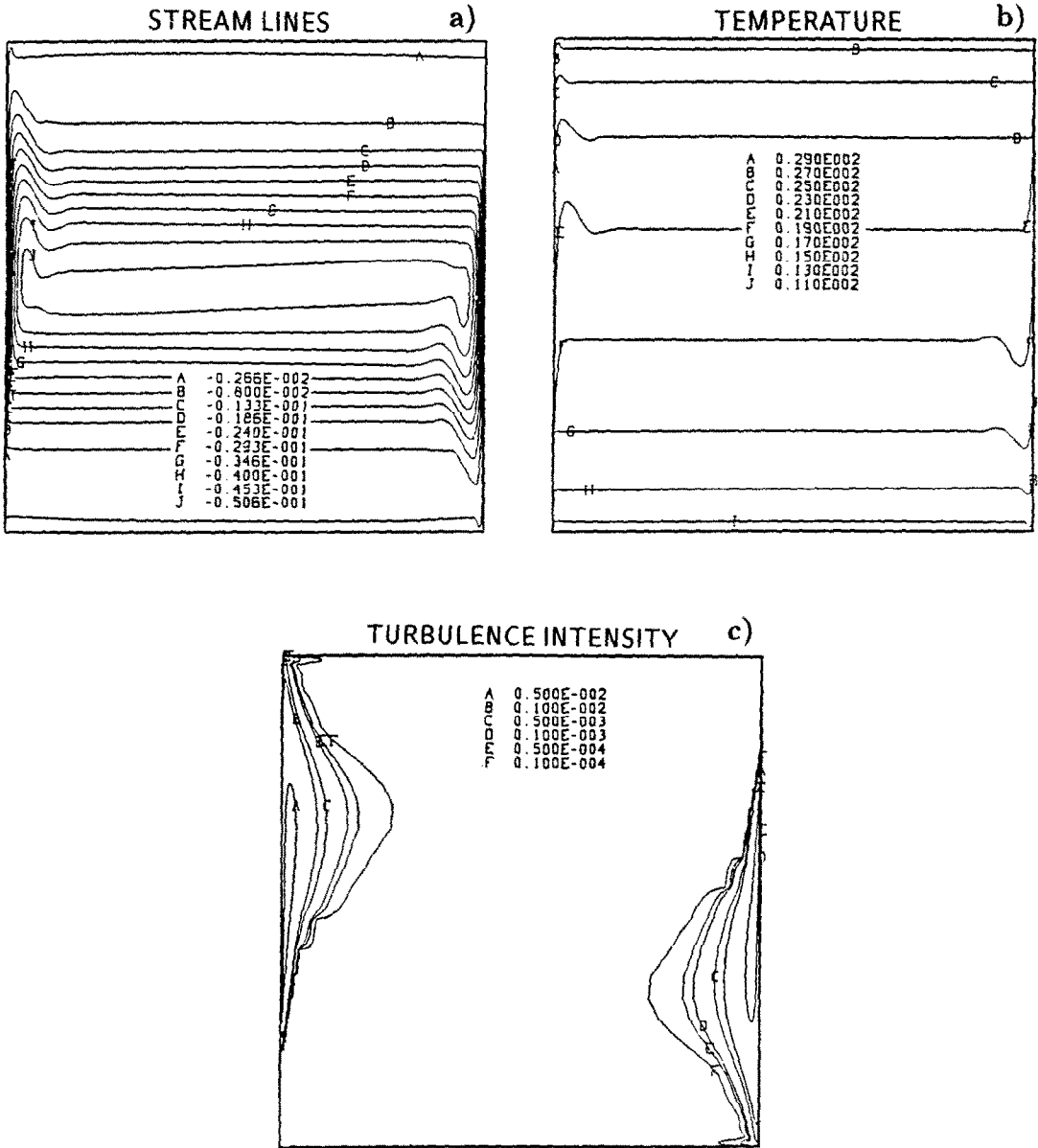


FIG. 6. Flow and temperature field in a square cavity at  $Ra = 10^{12}$ : (a) streamlines; (b) isotherms; (c) turbulence intensity.

into contact with the warm wall. A sharp decrease follows so that the  $Nu$  number falls practically to zero in the upper corner. For the three higher  $Ra$  numbers the profiles show a change of the gradient—an increase of  $Nu$ —at various positions, corresponding to the laminar-to-turbulent transition. In the case of  $Ra = 5 \times 10^{10}$  the transition is hardly visible and occurs roughly at  $y/H = 0.4$ , while in the case of  $Ra = 10^{12}$ , the transition is conspicuous and occurs at  $y/H = 0.2$ .

We also carried out the computations for the same cavity by using the three versions of the eddy diffusivity

models as described in Section 4.2. The obtained mean temperature and vertical velocity profiles show a very similar behaviour. The SGD model yielded a somewhat lower turbulence level as expected while GGD, PGD and AFM gave only marginal non-systematic differences.

To illustrate the effect we compare the averaged Nusselt numbers obtained with different models with the correlation  $Nu = C Ra^{1/3}$ , which has been generally accepted in literature as valid for the turbulent natural convection in cavities with thermally active vertical walls over a large span of  $Pr$  numbers and

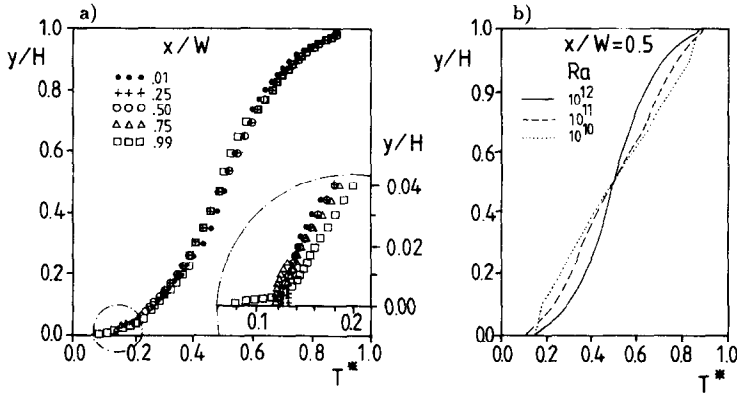


FIG. 7. Computed temperature profiles in vertical cross-sections; (a) for  $Ra = 10^{12}$ , with a blow up of the region adjacent to the adiabatic bottom; (b) influence of  $Ra$  number.

aspect ratios  $A$ .† As is well known, there is still no consensus on the value of the constant  $C$ , but most suggestions seem to fall between 0.043 and 0.047. So for instance, the experiments of McGregor and Emery [34] with cavities of aspect ratio from 1 to 40 and for  $Pr$  numbers from 1 to 20, with constant heat flux at the warm wall and isothermal cold wall (horizontal walls were adiabatic) for the range of  $Ra$  number of  $10^6$ – $10^9$  suggest that  $C = 0.046$  gives the best fit through the experimental data. In similar experiments with water in cavities of aspect ratio from 1.5 to 61, Cowan *et al.* [35] confirmed the same type of relationship, but found that for  $Ra = 2 \times 10^5$ – $2 \times 10^{11}$  the value of  $C$  should be 0.043. On the basis of an approximate theory of boundary layer on the vertical walls Raithby and Hollands [36] arrive at almost the identical result suggesting that  $C = 0.044$ . Numerical computations of Ince and Launder [13] for cavities of several aspect ratios between 1 and  $\infty$  indicate a marginal influence of  $A$ , and confirmed the above general correlation with  $C = 0.047$  approximating best the obtained results, except for  $A = \infty$ , for which  $C = 0.05$  seems a better value. On the basis of data of several authors for an infinite heated vertical plate, reduced to a square cavity with an assumption that the cavity core region is isothermal, Henkes *et al.* [17] also found that  $C = 0.047$ .

The difference between the mentioned values of the coefficient  $C$  is small and does not influence much the Nusselt number. However, the value of  $C$  reflects in a sense the position of the transition. If one assumes that for a laminar natural convection in a cavity at

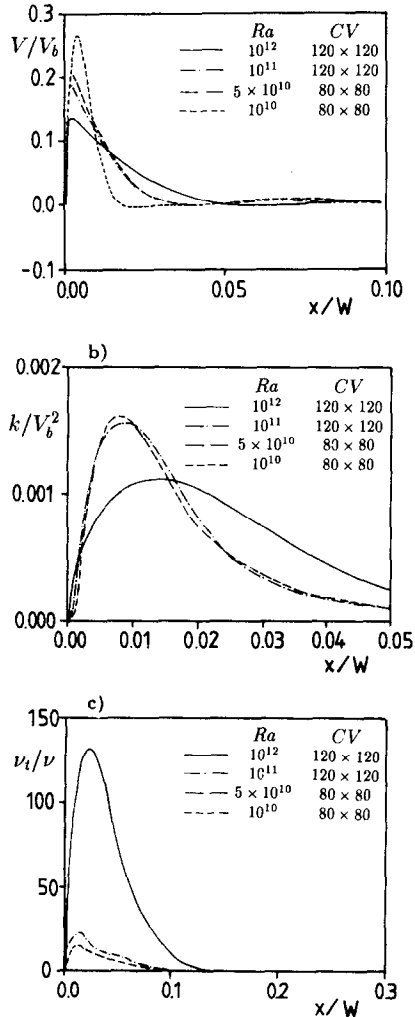


FIG. 8. Influence of  $Ra$  number on the computed profiles in the near-wall region at midheight: (a) vertical mean velocity; (b) turbulence kinetic energy; (c) normalized turbulent viscosity.

†The range of  $Ra$  numbers for which the correlation is claimed to be valid often includes values far below the critical  $Ra$  number, implying that the same correlation is valid for the laminar regime, contrary to the findings of some other authors, see Section 5.3.

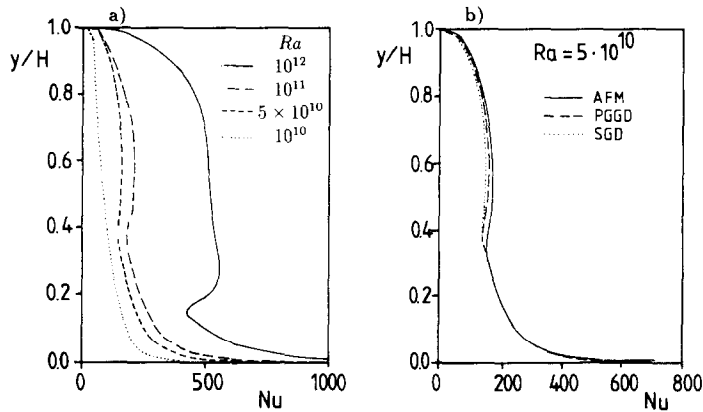


FIG. 9. Nusselt number along the isothermal walls: (a) influence of  $Ra$  number; (b) comparison of different turbulence models.

higher  $Ra$  numbers the heat transfer correlation can be expressed as  $Nu = C_l Ra^{1/4}$ , as suggested by some authors (see Gebhart *et al.* [1], pp. 750–751)† at the intersection of the two lines—representing the laminar and turbulent correlation—in a  $Nu$ – $Ra$  diagram, may be conditionally regarded as corresponding to the critical  $Ra$  number,  $Ra_{cr}$ , at which the laminar-to-turbulent transition occurs. It follows that  $Ra_{cr} = (C_l/C)^{12}$ , and hence is sensitive to the values of  $C_l$  and  $C$ . Of course, the choice of  $C_l$  is equally uncertain. If we assume, for illustration, that  $C_l = 0.30$ , as suggested by Henkes *et al.* [17] for air, the critical  $Ra$  number varies between  $4.57 \times 10^9$  for  $C = 0.047$  to  $1.33 \times 10^{10}$  for  $C = 0.043$ . Of course, a real critical  $Ra$  number will occur at somewhat higher values than those corresponding to the crossing point of the two correlations. Figure 10 shows the above relationship for  $C_l = 0.30$  (for air) and  $C_l = 0.32$  (for water) as suggested in ref. [17]. Most observations and computations suggest that for air, the transition occurs at  $Ra$  just above  $10^{10}$  and at a slightly higher value for water, suggesting that more appropriate are higher values of the coefficient  $C$ , say about 0.046–0.048. Our computations with various turbulence models yielded almost constant values of  $C$  independent of  $Ra$  in the considered range between  $10^{10}$  and  $10^{12}$ , but dependent on the chosen model. So for instance, the application of standard low  $Re$  number  $k$ – $\epsilon$  model of Launder and Sharma yielded for a square cavity an averaged value of  $C = 0.044$  (in fact  $C = 0.0447$  for  $Ra = 10^{10}$  and 0.0436 for  $Ra = 10^{12}$ ). The model with lateral temperature gradient replacing the streamwise one in the expression for the vertical heat flux with Yap correction yielded an averaged value of 0.0456, while the present algebraic model

gave  $C = 0.0483$ . In light of the previous discussion we regard the latter result as more accurate.

### 5.2. High aspect ratio rectangular cavities with side heating and cooling

We now turn to the cavity with a 5:1 aspect ratio. Experimental investigation of this geometry by Cheeswright *et al.* [31–33] constitute a good experimental basis for validation of the models and computation codes. As in the case of a square cavity, we carried out the computations by the same three versions of the eddy diffusivity model in addition to the present algebraic model. The computations were made by using a staggered, non-uniform grid of  $60 \times 60$  control volumes, as well as a finer grid with  $80 \times 100$  CV, which produced almost the same quality of results.

Validation of the computations were made on the basis of comparison with experimental data at the cavity midheight cross-section which showed to be a sensitive test for the turbulence models. As the results showed, both the standard SGD model and GGD model produced laminar-like solutions with a high peak and a steep gradient of the vertical mean velocity

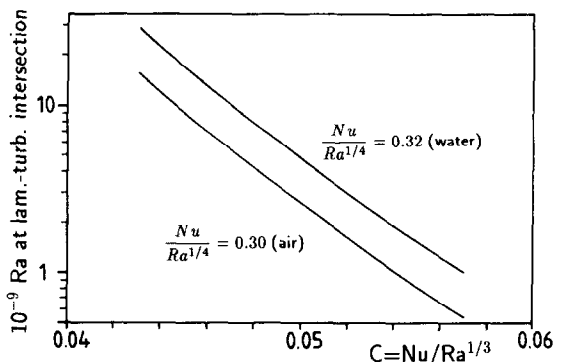


FIG. 10.  $Ra$  number at the intersection of laminar and turbulent heat transfer correlations for air and water.

† Our computations seem to approach this correlation only at  $Ra$  higher than  $10^8$ , while for lower  $Ra$  number the exponent is about 0.29, as discussed earlier.

in the wall region, as illustrated in Fig. 11(a). Because the turbulence level is small, the effects of Yap correction as well as of  $C_{\epsilon 3}$  is insignificant. Only after we omitted the streamwise gradient (PGGD model) did the solutions approach close to those reported by Ince and Launder [13], but with a slightly higher peak of the vertical velocity close to the warm wall, Fig. 11(b). Surprisingly, we did not notice much of an effect of the Yap correction. It was only after we changed the value of the coefficient  $C_{\epsilon 3}$  from 1.44 to 0.8 that the effect of Yap correction became visible. Indeed, in this case the solution without the correction of Yap was 'too turbulent' and this correction brought the results

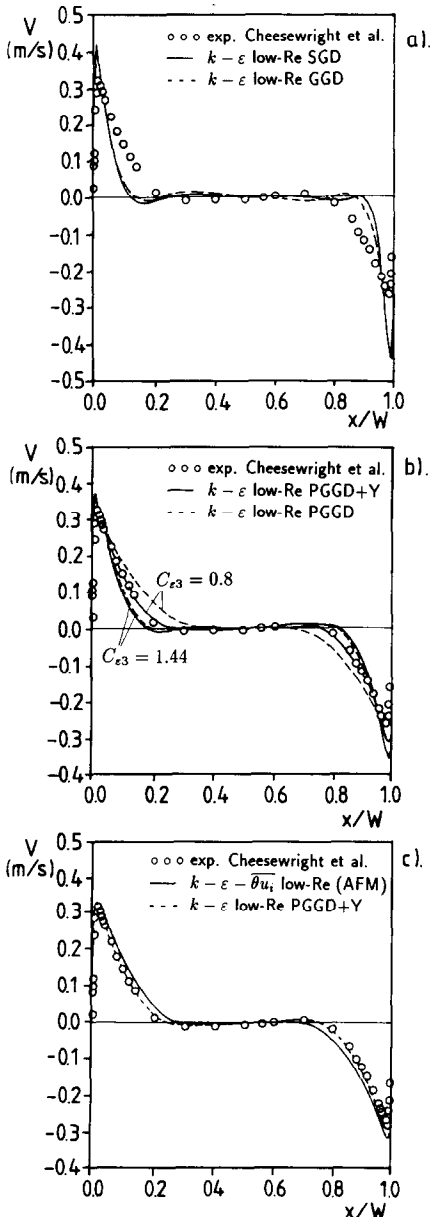


FIG. 11. Vertical velocity profiles at midheight of 5:1 cavity: comparison of different turbulence models.

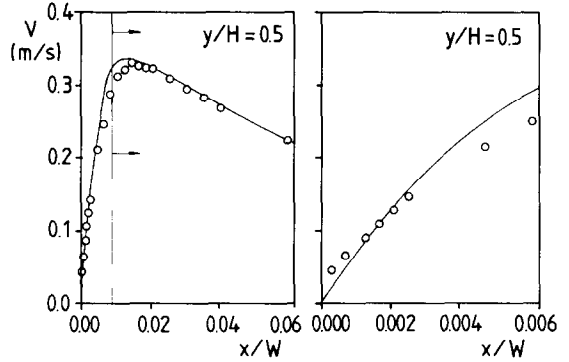


FIG. 12. Distribution of the vertical mean velocity close to the hot wall at midheight in 5:1 cavity:  $\circ$  experiments of Cheesewright *et al.* [31], — computations.

into a very good agreement with the experimental data.

The results obtained with the algebraic flux model AFM are shown in Fig. 11(c). As can be seen, the quality of agreement with the experiments is acceptable, though slightly inferior in comparison with those obtained by PGGD model with Yap correction. The agreement is in particular very good in the near-wall region as shown in detail in Fig. 12. Excellent agreement between the measured and computed velocity slope at the wall yielded a good prediction of the wall shear stress at this position. A plot of the distribution of the wall shear stress along the heated walls, Fig. 13, does not, however, reflect the same quality of agreement at all positions. The results for the cold wall are plotted for convenience upside down so that the computed curves collapse into one, reflecting an ideal symmetry of the flow. This symmetry has obviously not been achieved in the experiment. As reported by the authors, the flow rate along the cold wall was smaller than along the warm wall due to some downward flow along the lateral walls. However, unsatisfactory agreement with the data along the warm wall (which were, in fact, simulated

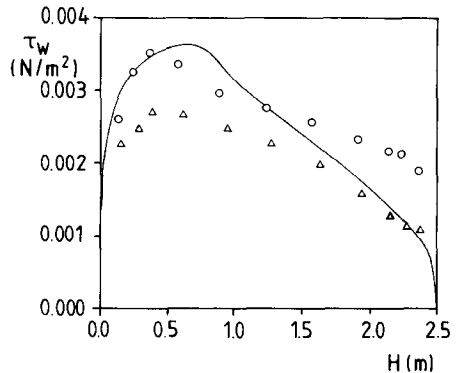


FIG. 13. Distribution of shear stress along the hot and cold walls of 5:1 cavity.  $\circ$  Experiments of Cheesewright and King [33], hot wall;  $\triangle$  cold wall; — computations.

by the computations), cannot be fully explained. Reported difficulties and inherent uncertainties in measuring the velocity very close to the wall, from which the wall shear stress was deduced, are most probably one of the causes for the disagreement. The other source of discrepancy may come due to some uncontrolled loss of heat at the top wall, as reported by the authors, which can cause a deformation of the velocity profile along the upper region of the warm vertical wall, as compared with the computed ideally adiabatic top wall conditions.

The variations of the mean temperature across the cavity at its midheight cross-section (not shown here) confirm a very good agreement in the near-wall region. In the core the computations yielded almost uniform temperature of 45°C, which is exactly half of the temperature difference between the warm and cold wall (68 and 22°C, respectively) reflecting an ideal symmetry. The experiments, however, showed about a 10% lower value. The disagreement, found also by Ince and Launder, probably has its origin in an uncontrolled heat loss through the later walls, as admitted by Cheesewright and King [33] and Cheesewright *et al.* [31].

It should be recalled that the algebraic flux model given by equations (11) and (12) contains all temperature and mean velocity gradients. Although the lateral temperature gradient is dominant in the buoyant generation of turbulence, in particular along the initial portion of the cavity vertical wall (where at the considered  $Ra$  numbers laminar-to-turbulent transition occurs), the streamwise gradient also seems to play an important role. In addition, it could be inferred from the measurements of Cheesewright *et al.* [31] that around the maximum of  $\overline{\theta u_1}$  the term  $\overline{\theta u_1}(\partial U_2/\partial x_1)$  amounts to at least 10% of the major generation term  $\overline{u_1 u_2}(\partial T/\partial x_1)$  in the region of peak  $\overline{u_1 u_2}$ . A similar order of magnitude has the term  $\overline{\theta u_2}(\partial U_2/\partial x_2)$ , because the peak  $\overline{\theta u_2}$  is about three times larger than that of  $\overline{\theta u_1}$ . Taking into account that the positions of the maxima of  $\overline{\theta u_1}$ ,  $\overline{\theta u_2}$  and  $\overline{u_1 u_2}$  are not coincident, it could be concluded that the strain rate part of the turbulent flux is not negligible. One should also bear in mind that the fluid in the inner wall layer (between the wall and the velocity maximum) accelerates until the transition occurs and then reduces to a turbulent profile with a smaller peak. Depending on the cavity aspect ratio it can accelerate further, but then it will decelerate as the end wall is approached. In the outer region the fluid will accelerate up to roughly midheight and then start to decelerate. All this will cause changes in the sign of the streamwise gradient of the vertical velocity, contrary to the streamwise gradient of the mean temperature, which remains monotonic. It is hard to conceive that all these peculiarities in the behavior of the exact terms in the differential equation for the turbulent heat flux can be imitated by a simple eddy diffusivity hypothesis. A success of the PGGD model seem to be more a coincidence which may come from mutual canceling

of the terms containing the streamwise gradients of the temperature and vertical velocity, which—in the inner layer at side wall just after the transition—have a same order of magnitude, but opposite signs.

A further support for this conclusion may be found in an inspection of the computed shear stress  $\overline{u_1 u_2}$  and turbulent heat flux components  $\overline{\theta u_1}$  and  $\overline{\theta u_2}$ , shown in Figs. 14(a)–(c) at the cavity midheight. Presented are the experimental data and the computations obtained with PGGD+Y model (dotted line) and with the AFM. The computed turbulent shear stress and the heat flux components did not show, however, the same quality of agreement. As can be seen in Fig. 14(a) the predicted  $\overline{u_1 u_2}$  (in both cases the same eddy viscosity hypothesis was used) at the midplane has a

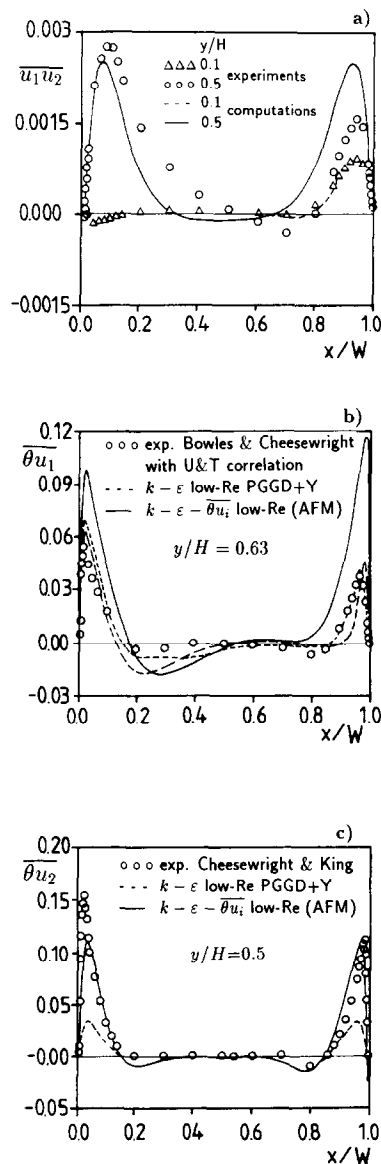


FIG. 14. Turbulence correlations at midheight of 5:1 cavity: (a) shear stress; (b) horizontal heat flux; (c) vertical heat flux.

similar shape and a same order of magnitude, as obtained by Cheesewright and King [33]. Here it should be noted that these experimental  $\overline{u_1 u_2}$  data were not measured directly, but estimated from the integration of the mean momentum equation across the boundary layer by feeding the measured mean velocity profiles. Several approximations were introduced which limit the analysis to the midheight region far away from the corners. Even here, some approximations are questionable, such as a neglect of the pressure gradient. Because of the lack of diagonal symmetry of the mean velocity profile, the evaluated data for  $\overline{u_1 u_2}$  of Cheesewright and King show an appreciable asymmetry. Since the integrals of both profiles of the shear stress across the cavity seem to be very close, it could be expected that fully symmetric boundary conditions in the experiment would produce the  $\overline{u_1 u_2}$  profile much closer to that obtained by our computations. The comparison of  $\overline{u_1 u_2}$  at  $y/H = 0.1$  in the same figure shows that the computations agree very well with the experimental data except close to the warm wall where the computed level of the turbulent stresses is negligible. At  $y/H = 0.9$  (not shown here) the disagreement is very large. While the computations gave an almost anti-symmetric profile, the experiments show a remarkable lack of any symmetry with very high values of experimentally obtained  $\overline{u_1 u_2}$ , which is difficult to justify. Inadequacy of the method used by Cheesewright and King [33] for corner region may be the source of error, but this would reflect also in the estimation of  $\overline{u_1 u_2}$  at  $y/H = 0.1$ , which, as shown earlier, agreed well with our computations. It is likely that the major source of error comes from the mean velocity profile which at this position was much affected by the earlier mentioned heat loss at the top wall. The quality of agreement of the  $\overline{u_1 u_2}$  profiles at the considered positions reflects the agreement between the computed and estimated wall shear stress, shown in Fig. 13. Nevertheless, it could be concluded that the comparison justifies the use of the simple eddy viscosity formula for computing the shear stress, at least at the region around the cavity midplane.

The agreement between the measured heat flux components and those computed by the PGGD+Y models are considerably poorer. Figure 14(b) shows a comparison of the data of Bowles and Cheesewright [32]—measured directly by a LDA and a thermocouple—of the horizontal heat flux component  $\partial u_1$  and those computed at the position slightly above the midplane at  $y/H = 0.63$  (experimental data for the midplane were not available). The predictions close to the hot wall agree reasonably well with the measurements, while those at the cold wall show a higher discrepancy. Bowles and Cheesewright admitted that the measured data are not free from error because the laser beam had to be angled toward the wall. However, their calculation from an integral balance applied to the measured data of Cheesewright and King produced a similar profile, suggesting that the

data have a realistic shape and order of magnitude. In light of the mentioned asymmetry in the experiment, the satisfactory agreement of the computed and measured data at the hot wall may be regarded more as a coincidence.

However, a striking disagreement appears between the computed (by PGGD+Y model) and measured profiles of the vertical heat flux component  $\partial u_2$ , as shown in Fig. 14(c). As discussed earlier, this flux component plays the principal role in the dynamics of turbulence kinetic energy in buoyant flows and influences directly the overall predictions of all quantities. The computed peak values in the wall vicinity are four to five times smaller than the measured ones. It is therefore more than surprising that the excellent agreement was achieved in mean velocity and temperature profiles, while the most important heat flux component was predicted very poorly.

The computations by the algebraic expressions (11) and (12) yielded considerably higher values of both heat flux components across the whole cavity cross-section, as seen in Figs. 14(b) and (c) (solid lines). And, while the horizontal heat flux was much over-predicted, the obtained vertical heat flux came to a close agreement with the measured data.

In fact, an inspection of the turbulence field, illustrated in Fig. 15 by contours of the normalized turbulent viscosity  $v_t/v$ , shows a concentration of turbulence with  $v_t/v$  reaching a value of about 100 at  $y/H = 0.75$  at the warm wall (and, symmetrically, at  $y/H = 0.25$  at the cold wall). At the cavity midplane at  $y/H = 0.5$  the ratio  $v_t/v$  is about 70, but the gradients of the turbulent viscosity are considerable. Hence, the solutions in the central region of the cavity height will be sensitive to even small changes in the applied model which will cause a shift of the eddy viscosity gradients up or down, without affecting much the maximum turbulence levels in the upper right and lower left corners.

An argument in favour of this conclusion is the finding that the earlier discussed eddy diffusivity models, which failed to produce acceptable results at the cavity midplane, yielded similar profiles of the vertical mean velocity at  $y/H = 0.25$  and  $0.75$  as well as at  $y/H = 0.1$  and  $0.9$  (not shown where), as the PGGD and AFM models.

The computations of Nusselt numbers for three values of  $Ra$  numbers  $10^{10}$ ,  $10^{11}$  and  $10^{12}$  follow very well the correlation  $Nu = C Ra^{1/3}$  with  $C = 0.048 \pm 0.001$ , which agrees with our findings for a square cavity. This confirms the conclusions of Ince and Launder [13] that the aspect ratio has no significant influence upon the heat transfer correlation at least in the considered range of  $A = 1-5$ .

### 5.3. Heat transfer correlation for side heated cavities—some further remarks

It is worth mentioning at this point that some results reported in the literature do not follow the heat transfer correlation  $Nu = C Ra^{1/3}$ , as also shown in Fig. 16.

The data of Bauman *et al.* [37], obtained with water in a cavity with aspect ratio  $A = 0.5$  and for  $Pr = 2.6-6.8$  for a relatively narrow range of  $Ra$  number of  $2-6 \times 10^{10}$ , in spite of a considerable scatter, follow a

different  $Nu-Ra$  number dependence with an exponent of  $Ra$  visibly smaller than  $1/3$ . It is interesting to note that the experiments of Nansteel and Grief [38] with a cavity of the same aspect ratio  $A = 0.5$ , but with a partial vertical division hanging from the ceiling, obtained a correlation with a similar slope,  $Nu = 0.762Ap^{0.473}Ra^{0.226}$  ( $Ap$  is the aperture ratio) for  $Ra$  between  $2 \times 10^{10}$  and  $1.1 \times 10^{11}$ , but their values of  $Nu$  numbers for a case without partition,  $Ap = 1$ , exceed those of Bauman *et al.* by about 17%. To this group of results one may add the experimental correlation  $Nu = 0.62Ra^{0.25}$  of Bohn *et al.* [39] obtained in a cubical cavity with several combinations of heating and cooling of vertical walls, while the horizontal walls were kept adiabatic. The case with the two neighboring vertical walls heated and the other two walls cooled (HHCC combination) could be compared with the presently considered case of square cavity with opposite walls heated and cooled if the coefficient in the above correlation is divided by two as to match the corresponding temperature difference between the warm and cold walls. The resulting correlation (with the coefficient  $C = 0.31$ ), shown also in Fig. 16, follows a similar slope as that of Nansteel and Grief, and Bauman, but yields considerably smaller values of  $Nu$  numbers (e.g. for  $Ra = 10^{11}$  this difference is about  $-13\%$ ). A common feature of all three cases is that no turbulence was detected, although the  $Ra$  numbers were high. The small aspect ratio of 0.5 in both Bauman, and Nansteel and Grief cases may be the reason for persistence of laminar regime at such high  $Ra$  numbers, but these findings as well as the discrepancy in magnitudes of  $Nu$  numbers need further clarification.

Figure 16 shows a graphical comparison between results of various authors together with our computations.

5.4. Cavities with mixed boundary conditions

In most real situations the boundary conditions are usually of a mixed type, and often non-uniformly distributed. Kirkpatrick and Bohn [2] carried out detailed measurements and flow visualization tests of free convection in a cubical enclosure with an interior dimension of 0.305 m filled with deionized water. Four different configurations of boundary conditions were generated by exposing the top wall and two of the side walls to heating and cooling in different combinations, while keeping the bottom wall heated and the remaining two opposite side walls insulated. We present here the comparison of the numerical results with the experimental data for one of the cases, namely the case denoted as HHCC with heated bottom and left side wall and cooled top and right side wall. The heated walls were kept at  $45^\circ\text{C}$  and the cooled ones at  $15^\circ\text{C}$  so that the cavity configuration has a diagonal symmetry with reference bulk temperature of  $30^\circ\text{C}$ .

As found earlier, the standard low  $Re$  number  $k-\epsilon$  model produced in a square cavity almost the same quality of agreement as the more complex algebraic

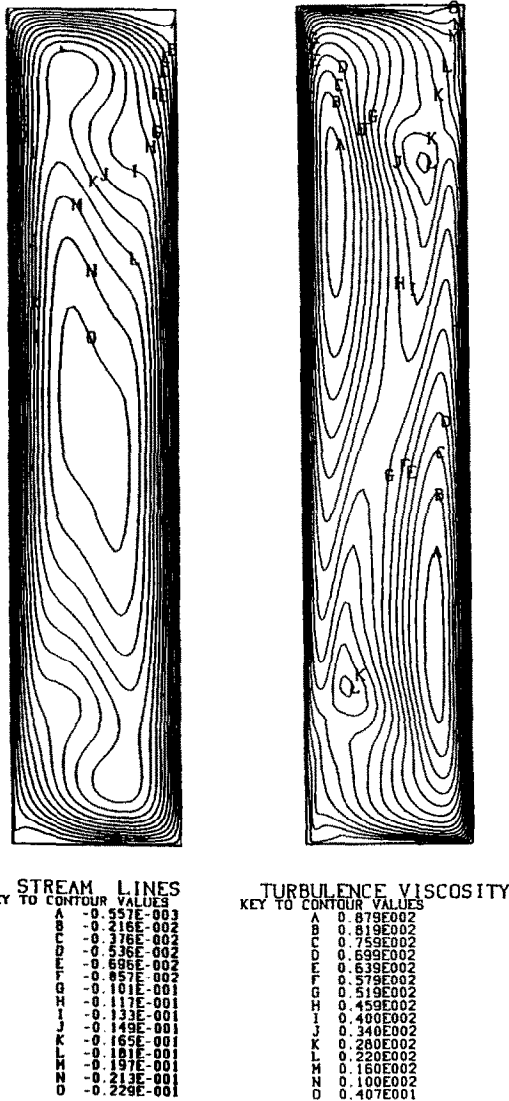


FIG. 15. Streamlines and contours of turbulent viscosity in a 5:1 cavity.

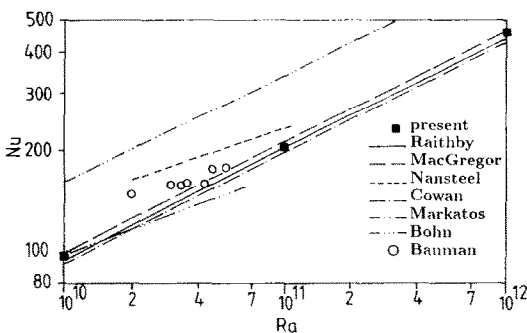


FIG. 16. Heat transfer correlation: comparison of different experimental data and computations.

model, yielding only a slightly lower level of turbulence and consequently lower averaged  $Nu$  numbers. We discuss here the results for a square cavity with mixed boundary conditions, obtained by the simpler model and SGD hypothesis.

The numerical grid with  $80 \times 80$  CV was non-uniformly distributed and squeezed in the wall region so that at least 12 points fall between the wall and maximum velocity, and with the first grid point placed at  $y^+$  less than 0.5. Figure 17 show in sequence the velocity vector field (a), streamlines (b) as well as profiles of the turbulent  $Re$  number at several vertical cross-sections (c). The flow pattern agrees well with that recorded by flow visualization. As can be seen, the flow rotates in the clockwise direction with an intensive motion within the boundary layers along the walls. Gravitational force disturbs the diagonal symmetry generating thicker boundary layers at horizontal walls than on vertical ones. Intensive fluid circulation due to the differential heating of the vertical walls generates an almost isothermal core and prevents the appearance of thermals which characterize the unstably stratified field with bottom heating and top wall cooling. In the left corner the flow visualization indicated the appearance of small thermals, which cannot be predicted by the present method, but the overall agreement between the streamline patterns is satisfactory. These thermals are carried away by the side wall boundary layer so that they rise against the pressure gradient into the upper left corner of the cavity without much exchange of heat with the surrounding fluid. Colder than fluid within the boundary layer, the thermals are unable to penetrate fully into the stratified boundary layer on the upper wall; they decelerate and form a vortex in the upper left zone of the cavity (denoted by the streamline H in Fig. 17(b)). For the same reason a similar but cold vortex appears in the lower right region of the cavity. The velocity vector plot, Fig. 17(a), as well as velocity profiles (not presented here) show that the maximum velocities on the vertical walls appear very close to the walls while on the horizontal walls the maximum velocity is closer to the contact of the heated and cooled walls. As a consequence of such a flow pattern, the central region of the cavity is filled with the central vortex, which rotates in the counterclockwise direction, Fig. 17(b).

The temperature profiles reflect in the whole the flow pattern described above, as shown in Figs. 18(a)–(c), except that the thermal wall boundary layers are considerably thinner. This is particularly pronounced on the vertical profiles of temperature at positions close to the vertical walls (not visible in Fig. 18). Unfortunately, the experimental data of Kirkpatrick and Bohn do not yield possibilities for more detailed verification of the computed data. The only possibility for comparison is the temperature profile at the mid position which is presented in Fig. 18(c). As seen, both the computed and measured profiles show the same qualitative behavior, though the quantitative agreement is not fully satisfactory. The difference is

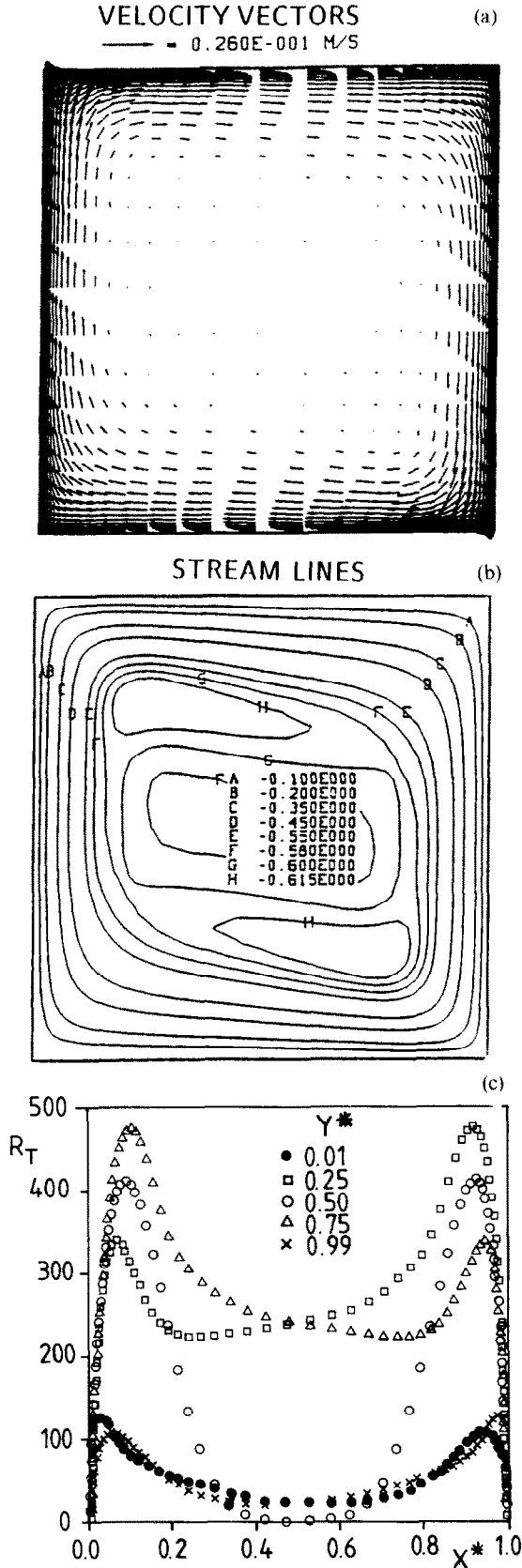


FIG. 17. Velocity vectors, streamlines and profiles of turbulence Reynolds number in a square cavity with bottom and side heating—top and side cooling.

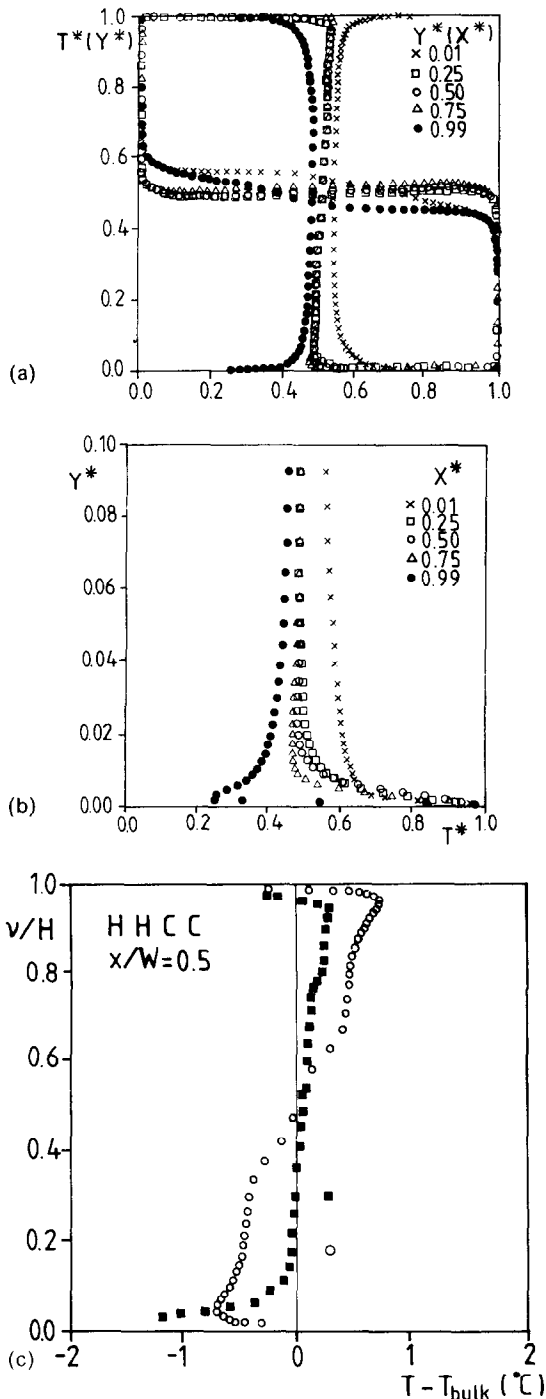


FIG. 18. Normalized profiles of mean temperature at different horizontal and vertical cross-sections in a square cavity with bottom and side heating—top and side cooling. ■ Experiment (Kirkpatrick and Bohn [2]), ○ Computations.

only about 0.5 C (note the expanded scale of  $T - T_{\text{bulk}}$  on abscissa), i.e. the experimental data show a total variation of core temperature with respect to  $T_{\text{bulk}}$  within 0.5 C while the computed results yield a variation within 1.0 C. Hence the experiments indicate a more intensive vertical mixing than predicted by the numerical model. Of course, the difference between

the experiments and computations is so small that it could also be attributed to the imperfection of the experiment, i.e. three-dimensionality, wall radiation, non-uniformity of the wall temperatures, etc. The same effects could be blamed for a disagreement noticeable very close to the bottom wall. The measurements show here a higher subcooling of the fluid below the bulk temperature by 1.2 C, while the maximum computed temperature difference is 0.8 C. The measurements could not be carried out very close to the wall where the fluid temperature steeply approaches the wall value of 15 C. Hence no detailed comparison of the computations was possible in the near-wall region.

Kirkpatrick and Bohn proposed also the  $Nu-Ra$  number correlations separately for each pair of walls. For the considered HHCC configuration they found that the experimental data for the top and bottom walls fit best the relationship  $Nu = 1.1 Ra^{0.236}$ , while for the vertical walls the proposed correlation is  $Nu = 0.141 Ra^{0.313}$ . In both correlations the  $Ra$  number was based on the difference in temperatures of the warm and cold wall,  $T_h - T_c$ , while the  $Nu$  number was defined with the difference between the wall temperature and the bulk temperature  $T_{\text{bulk}}$ . The latter is defined as the arithmetic mean of the temperatures of all four walls. The authors concluded that the first correlation is not much affected by the imposed horizontal temperature difference. However, the second correlation yields higher values of  $Nu$  at the vertical walls if there is a bottom heating because the raising thermals are supposed to enhance the heat transfer also on the vertical walls.

Our computations at  $Ra = 2.15 \times 10^{10}$ —defined as above—yielded  $Nu$  numbers for horizontal walls of 254 which is about 16% smaller than the value 302 obtained from the above experimental correlation of Kirkpatrick and Bohn. Likewise, for the vertical walls the computed  $Nu = 224$  is smaller by 7% than the experimental value of 242. Although a possible lack of control of the experimental boundary conditions, inherent in the above experimental correlations, but not accounted for by the numerical computations, may be a source of discrepancy, the differences are too large to be attributed to the imperfection of the experiment. It seems more likely that the applied low  $Re$  number  $k-\epsilon$  model with SGD hypothesis is inadequate for predicting accurately the considered configuration. It is symptomatic that this model produced again lower values of Nusselt numbers at both vertical and horizontal walls, as detected in the two cases discussed in previous Sections.

The discrepancy is somewhere in between those found for the square and tall cavity with side heating and cooling. Lower values of  $Nu$  numbers obviously reflect a too low turbulence level predicted by the SGD model. It is expected that the algebraic model will bring the results in closer agreement with reality. Of course, none of the models can predict thermals nor any other large scale coherent motion. However, as mentioned before, the average effects including the

heat transfer on horizontal heated plate has been accounted for to a satisfactory level of agreement with experiments with the improved algebraic model of turbulence. A further study of this case would require more detailed experimental data for the model comparison and verification than presently available.

## 6. CONCLUSIONS

In a search for an adequate model for the computation of complex buoyancy dominated turbulent flows with arbitrary boundary conditions a form of algebraic flux model was derived and its performance tested on the computation of several types of external and confined buoyancy-driven motion. Results for natural convection in rectangular enclosures with different aspect ratios and boundary conditions are discussed with parallel referencing to earlier reported computations of free convection on the walls heated from the side and from below. It was found that the low  $Re$  number  $k$ - $\epsilon$  transport equations can be employed to describe the evolution of buoyancy affected turbulence and its scales, provided that the adequate formulation of the turbulent heat flux is used to represent the buoyant production. Since the mechanical production of turbulence is dominated by shear within the wall boundary layers, the results did not show much sensitivity to the formulation of turbulent stresses and, for the sake of simplicity, the standard eddy viscosity representation was retained with  $f_\mu$  and  $f_\epsilon$  functions of Launder and Sharma.

The major conclusion concerns the modeling of the turbulent heat flux vector which was found to influence strongly the applicability of the model to a broader class of buoyant flows. Variants of gradient diffusion model with isotropic and non-isotropic eddy diffusivity and corresponding components of temperature gradients, were found to produce results of inconsistent quality. By contrast, the algebraic model of turbulent heat flux—derived by a straightforward truncation of the modeled differential transport equation, with constant values assigned to the coefficients  $\Phi_\theta$  and  $C_\theta^0$ —produced satisfactory results for all considered cases.

Specifically, it was found that in a square cavity with side heating and cooling, results obtained with different models are reasonably close to each other. Differences appear in the case of tall cavities with the same boundary conditions where the development length of the boundary layers along the vertical walls is more influential. The same is the case for cavities, with simultaneous heating from sides and from the bottom. In both latter cases the effects of other terms, not accounted for by the eddy diffusivity models, which represent the interaction between the turbulent stresses and heat flux component with the mean temperature field and with mean rate of strain, are not negligible, in particular in the range of  $Ra$  number around and just after the laminar-to-turbulent transition.

Reliable computations of specific features of buoyant flows will eventually require the application of a model at a second moment closure level. It is believed, however, that the described algebraic flux model (AFM) could serve for the computation of complex buoyancy driven flows in various geometries and with mixed boundary conditions—at least in the interim—until the uncertainties inherent in higher order models and difficulties in implementing these models into a general Navier–Stokes code are resolved.

*Acknowledgements*—This work was sponsored by the Science Fund of Bosnia and Herzegovina. A part of the computations and the final writing of the paper were carried out at the Lehrstuhl für Strömungsmechanik of the Friedrich-Alexander Universität Erlangen-Nürnberg. The first author acknowledges with thanks the award of DFG guest professorship which enabled him an extended stay at LSTM. Fruitful interactions with Prof. F. Durst and Dr M. Perić from the Friedrich-Alexander University and Prof. I. Demirdžić from the University of Sarajevo are also acknowledged.

## REFERENCES

1. B. Gebhart, Y. Jaluria, R. L. Mahajan and B. Sammakia, *Buoyancy-induced Flows and Transport*. Hemisphere, New York (1988).
2. A. T. Kirkpatrick and M. Bohn, An experimental investigation of mixed cavity natural convection in the high Rayleigh number regime, *Int. J. Heat Mass Transfer* **29**, 69–82 (1986).
3. S. Ostrach, Natural convection in enclosures, *J. Heat Transfer* **110**, 1175–1190 (1988).
4. B. E. Launder, On the computation of convective heat transfer in complex turbulent flows, *J. Heat Transfer* **110**, 1112–1128 (1988).
5. T. W. J. Peeters and R. A. W. M. Henkes, The Reynolds-stress model of turbulence applied to the natural-convection boundary layer along a heated vertical plate, *Int. J. Heat Mass Transfer* **35**, 403–420 (1992).
6. M. P. Fraikin, J. J. Portier and C. J. Fraikin, Application of a  $k$ - $\epsilon$  turbulence model to an enclosed buoyancy driven recirculating flow, *ASME A.I.Ch.E. Natn. Heat Transfer Conf.*, Orlando, Florida (1980).
7. N. C. Markatos and K. A. Pericleous, Laminar and turbulent natural convection in an enclosed cavity, *Int. J. Heat Mass Transfer* **27**, 755–772 (1984).
8. H. Ozoe, M. Mouri, M. Ohmuro, S. W. Churchill and N. Lior, Numerical calculation of laminar and turbulent natural convection in water in rectangular channel heated and cooled isothermally on the opposing vertical walls, *Int. J. Heat Mass Transfer* **28**, 125–138 (1985).
9. C. P. Thompson, N. S. Wilkes and I. P. Jones, Numerical studies of buoyancy driven turbulent flow in a rectangular cavity, *Int. J. Num. Meth. Engng* **24**, 89–99 (1987).
10. T. Fusegi and B. Farouk, Laminar and turbulent natural convection-radiation interaction in a square enclosure filled with a nongray gas, *Numer. Heat Transfer* **15**, 303–322 (1989).
11. E. Nobile, A. C. M. Sousa and G. S. Barozzi, Turbulent buoyant flows in enclosures, *Proc. 9th Int. Heat Transfer Conf.* 543–548 (1990).
12. P. L. Betts and A. A. Dafa'Alla, Turbulent buoyant air flow in a tall rectangular cavity, *Proc. ASME Meeting HTD* **60**, 83–91 (1986).
13. N. Z. Ince and B. E. Launder, On the computation of buoyancy-driven turbulent flows in rectangular enclosures, *Int. J. Heat Fluid Flow* **10**, 110–117 (1989).
14. L. Davidson, Calculation of the turbulent buoyancy-

- driven flow in a rectangular cavity using an efficient solver and two different low- $Re$  number  $k$ - $\epsilon$  turbulence models, *Numer. Heat Transfer* **18**, 129–148 (1990).
15. P. W. Giel and F. W. Schmidt, A comparison of turbulence modelling predictions to experimental measurements for high Rayleigh number natural convection in enclosures, *Proc. 9th Int. Heat Transfer Conf.* **2**, 175–180 (1990).
  16. K. Hanjalić and S. Vasić, Numerical simulation of free convection in single- and multiple-zone rectangular cavities, *Proc. 9th Int. Heat Transfer Conf.* **2**, 579–584 (1990).
  17. R. A. W. M. Henkes, F. F. van der Vlugt and C. J. Hoogendoorn, Natural-convection flow in a square cavity calculated with low-Reynolds-number turbulence models, *Int. J. Heat Mass Transfer* **34**, 377–378 (1991).
  18. W. P. Jones and B. E. Launder, Prediction of laminarization with a two-equation model of turbulence, *Int. J. Heat Mass Transfer* **15**, 301–314 (1972).
  19. B. E. Launder and B. I. Sharma, Application of the energy dissipation model of turbulence to the calculation of flow near spinning disc, *Lett. Heat Mass Transfer* **1**, 131–138 (1974).
  20. M. Perić, Efficient semi-implicit solving algorithm for nine-diagonal coefficient matrix, *Numer. Heat Transfer* **11**, 251–279 (1987).
  21. G. De Vahl Davis, Natural convection of air in a square cavity: a benchmark numerical solution, *Int. J. Num. Meth. Fluids* **3**, 249–264 (1983).
  22. M. Hortmann, M. Perić and G. Scheuerer, Finite volume multigrid prediction of laminar natural convection: benchmark solutions, *Int. J. Num. Meth. Fluids* **11**, 189–207 (1990).
  23. V. I. Polezhaev, Mathematical modelling of convective heat and mass transfer in elements of heat and power generating systems, *Proc. Int. Forum on Math. Modelling and Computer Simulation of Processes in Energy Systems* (Edited by K. Hanjalić), Hemisphere (1990).
  24. H. Ozoe, M. Ohmuro, A. Mouri, S. Mishima, H. Sayama and S. W. Churchill, Laser Doppler measurements of the velocity along a heated vertical wall of a rectangular enclosure, *J. Heat Transfer* **105**, 782 (1983).
  25. S. M. Bajorek and J. R. Lloyd, Experimental investigation of natural convection in partitioned enclosures, *J. Heat Transfer* **104**, 527 (1982).
  26. K. Hanjalić and S. Vasić, Some further exploration of turbulence models for buoyancy driven flows. In *Turbulent Shear Flows 8* (Edited by F. Durst *et al.*), pp. 319–341. Springer, Berlin (1993).
  27. M. M. Gibson and B. E. Launder, On the calculation of horizontal nonequilibrium turbulent free shear flows under gravitational influence, *J. Heat Transfer* **98**, 81–87 (1976).
  28. T. Tsuji, Y. Nagano and M. Tagawa, Thermally driven turbulent boundary layer, flat plate, *Proc. 8th Symp. Turbulent Shear Flows* 24–3 (1991).
  29. W. M. To and J. A. C. Humphrey, Numerical simulation of buoyant, turbulent flow—I. Free convection along a heated, vertical, flat plate, *Int. J. Heat Mass Transfer* **29**, 573–592 (1986).
  30. S. Tavoularis and S. Corrsin, Experiments in nearly homogeneous turbulent shear flow with a uniform mean temperature gradient, *J. Fluid Mech.* **104**, 311–347 (1981).
  31. R. Cheesewright, K. J. King and S. Ziai, Experimental data for the validation of computer codes for the prediction of two-dimensional buoyant cavity flows, *Proc. ASME Meeting HTD* **60**, 75–81 (1986).
  32. A. Bowles and R. Cheesewright, Direct measurements of the turbulence heat flux in a large rectangular air cavity, *Exp. Heat Transfer* **2**, 59–69 (1989).
  33. R. Cheesewright and K. J. King, Stress distribution in natural convection in a rectangular air cavity, *Proc. 9th Int. Heat Transfer Conf.* **2**, 161–167 (1990).
  34. R. K. McGregor and A. F. Emery, Free convection through vertical plane layers—moderate and high Prandtl number fluids, *J. Heat Transfer* **91**, 391–403 (1969).
  35. G. H. Cowan, P. C. Lovegrove and G. L. Quarini, Turbulent natural convection heat transfer in vertical single water-filled cavities, *Proc. 7th Int. Heat Transfer Conf.* 195–204 (1982).
  36. G. D. Raithby and K. G. T. Hollands, A general method of obtaining approximate solutions to laminar and turbulent free convection problems, *Adv. Heat Transfer*, Academic Press, **11** (1975).
  37. F. Bauman, A. Gadghil, R. Kammerund and R. Grief, Buoyancy-driven convection in rectangular enclosures: experimental results and numerical calculations, ASME Paper No. 80-HT-66 (1980).
  38. M. W. Nansteel and R. Grief, Natural convection in undivided and partially divided rectangular enclosures, *J. Heat Transfer* **103**, 623–629 (1981).
  39. M. S. Bohn, A. T. Kirkpatrick and D. A. Olson, Experimental study of three-dimensional natural convection at high  $Ra$  number, *J. Heat Transfer* **106**, 339–345 (1984).